Radio Science, Volume 33, Number 4, Pages 861–893, July–August 1998

Stratosphere-troposphere ozone exchange observed with the Indian MST radar and a simultaneous balloon-borne ozonesonde

T. K. Mandal,[1] J. Y. N. Cho, [2,3] P. B. Rao,[4] A. R. Jain,[4] S. K. Peshin,[5]
S. K. Srivastava,[5] A. K. Bohra,[6] and A. P. Mitra[1]

Abstract. The stratosphere-troposphere (ST) mode operation of the Indian mesosphere-stratosphere-troposphere (MST) radar provided evidence of multiple stable layer structures near the tropopause and also of its "weakening" during late night hours on several occasions. Mass exchange can take place between the troposphere and the stratosphere during periods of such weakening. To examine whether there is any transport of ozone from the stratosphere to the troposphere at the time of tropopause weakening at tropical latitudes, simultaneous observations were carried out using the Indian MST radar located at Gadanki (13.5°N, 79.2°E), now fully operational in MST mode, and ozonesonde flights from Trivandrum (8.9°N, 76.6°E). Four campaigns of simultaneous observations were conducted during January 3-8, November 9-16, and December 5-10, 1994, and June 7-24, 1995. The results show occurrence of the tropopause weakening several times during January 3-8, November 9-16, and December 5-10, 1994. Simultaneous observations of ozone profiles, particularly on January 7-8, November 10 and 16, and December 7-8, 1994, the days of tropopause weakening, show evidence of a decrease in stratospheric ozone and a corresponding increase in tropospheric ozone after this event, the total ozone remaining essentially constant on these days with respect to other days. Tropopause weakening on January 4-5, 1994, however, does not show any considerable change in the ozone profiles. The results are presented here relating the degree of tropopause weakening to the extent of vertical mass exchange between the troposphere and the stratosphere. An effort has been made to examine the role of horizontal advection of ozone in increasing tropospheric ozone at the region of interest; the geographical distribution of tropospheric ozone residual (TOR) has been analyzed by the two data sets obtained independently from Meteor 3 total ozone mapping spectrometers (Meteor 3 TOMS) and the Upper Air Research Satellite (UARS). Simultaneously, the possibility of horizontal transport of ozone from the areas surrounding Tirupati and Trivandrum in increasing tropospheric ozone due to synoptic scale circulation has also been verified by close inspection of synoptic weather charts at 1000, 700, 500, and 300 hPa obtained from the National Center for Medium-Range Weather Forecasting general circulation model at 0000 and 1200 UTC on January 7 and 0000 and 1200 UTC on January 8, 1994.

[1]Radio and Atmospheric Division, National Physical Laboratory, New Delhi, India.
[2]Arecibo Observatory, Arecibo, Puerto Rico.
[3]Department of Earth, Atmospheric and Planetary Sciences, Massachusetts Institute of Technology, Cambridge.
[4]National MST Radar Facility, Tirupati, India.
[5]India Meteorological Department, New Delhi, India.
[6]National Center for Medium Range Weather Forecasting, New Delhi, India.

Paper number 97RS03553.
0048-6604/98/97RS-03553$11.00

1. Introduction

The downward flux of stratospheric ozone into the troposphere controls the tropospheric ozone budget in middle and high latitudes [*Danielsen and Mohnen*, 1977; *Fishman and Crutzen*, 1978]. Although representing only 10 % of the total column, tropospheric ozone is an important gas because it can influence the chemical cycles and lifetimes of many important trace gases (e.g., H_2O,CO, CH_4, H_2S, etc.) in the troposphere because of its photolysis by UV radiation in the presence of water vapor [*Wofsy et al.*,1972]. In addition, it is a greenhouse gas itself and can change the radiation budget and thus may affect the climate [*Ramanathan and Dickinson*, 1979].

Recently, *Suhre et al.* [1997] have observed high ozone concentrations in the upper equatorial Atlantic troposphere as a part of the Measurement of Ozone by Airbus In-Service Aircraft (MOZAIC) Experiment. Therefore the contribution of the downward vertical transport of stratospheric ozone to the background tropospheric ozone budget in the tropics is not clear.

It is now widely appreciated that the dynamics of the troposphere and stratosphere are, in principle, inseparable [e.g., *Hoskins et al.*, 1985]. The tropopause, the intermediate barrier between the stratosphere and troposphere, plays a crucial role in transport processes of air and chemical tracers on timescales as short as a few hours between these two regions [*Reiter et al.*, 1969]. In addition, latitudinal and seasonal changes in the tropopause are related to dynamical processes of different timescales and space scales of general circulation. The tropopause has been routinely observed for decades by radiosondes twice a day on a global basis. Climatological studies can be done on these data sets, but the dynamical processes of shorter timescales may not be followed by routinely observed radiosonde data. According to World Meteorological Organization (WMO) guidelines, the tropopause must be defined as the bottom of a layer thicker than 2 km with a mean lapse rate equal to or less than 2 K/km. *Bjerknes and Palmen* [1937] first observed the layered tropopause of a few kilometers thickness in vertical scale (10^2-10^3 km in horizontal extent and less than a day in temporal scale) with radiosonde data. So multiple structures in radiosonde temperature profiles with vertical scale of ~2 km are smoothed out according to WMO guidelines.

With the advent of clear-air Doppler radar it has become possible to continuously monitor this multiplicity structure near the tropopause under all weather conditions. The multiple layered structure near the tropopause was observed by stratosphere-troposphere (ST) mode operation of the Indian mesosphere-stratosphere-troposphere (MST) radar [*Jaya Rao et al.*, 1994] and has also been observed at other latitudes [*Dalaudier et al.*, 1994; *Yamanaka et al.*, 1996]. However, *Yamanaka et al.* [1996] proposed that the subtropical multiple tropopauses, for which layered turbulence generation is required in the tropopause region, are nothing but the dominant modes of lower stratospheric inertio-gravity waves. At higher latitudes, the occurrence of multiple tropopause structure may be due to frequent vertical exchange across the tropopause [*Mahlman*, 1997].

In addition, sudden changes in tropopause structure on timescales less than few hours or so have also been detected by MST radar at middle and high latitudes [*Rastogi and Rottger*, 1982; *Larsen and Rottger*, 1985; *Nastrom et al.*, 1989], and it is well documented as tropopause folding/break. Generally, rapid and irreversible mass exchange occurs between the stratosphere and troposphere during this period [*Danielsen*, 1968]. It may be associated with synoptic scale (mesoscale) features [*Nastrom et al.*, 1989]. Therefore the comparative time series analysis of radar data with weather maps and cross sections based on synoptic radiosonde data may help to interpret the mass transport from stratosphere to troposphere.

At midlatitudes the correlation between the synoptic scale circulation and well-documented tropopause folding/break and cutoff low in the upper troposphere has been already established during mass exchange [*Danielsen*, 1968; *Vaughan and Price*, 1989; *Bamber et al.*, 1984]. *Folkins and Appenzeller* [1996] and *Gouget et al.* [1996] reported mass exchange during the subtropical break/fold between 13°N and 23.5°N based on the diagnostic model analysis of meteorological wind fields. They have related the subtropical folding/break to the winter subtropical jet stream at 200 hPa obtained from European Centre for Medium-Range Weather Forecasting (ECMWF) analysis.

Dobson et al. [1929] first noticed the relationship between synoptic scale circulation and total ozone. Later, *Reed* [1950] proposed a model to describe the relationship between the total ozone and weather patterns for the northern hemisphere. The relationship between ozone amounts and day-to-day weather parameters is well documented in the literature [*Vaughan and Price*, 1989; *Ebel et al.*, 1991]. They have also found that near a cutoff low in the upper troposphere, the synoptic scale circulation has a good correlation with stratosphere-troposphere exchange, which determines the distribution of ozone in the atmosphere. *Shapiro et al.* [1982], *Ebel et al.* [1991], and *Uccellini et al.*, [1985] have also shown how the total ozone field obtained from total ozone mapping spectrometer (TOMS) is affected by position and intensity of jet streams and tropopause folding/break events in midlatitude and found good correlation with synoptic scale circulation. *Rodgers et al.*, [1990] have extended them to subtropics, where total ozone fields change with the tropical cyclones and tropopause topography.

Fishman et al. [1986] have shown that day-to-day total ozone variations are dominated by tropospheric ozone changes in the equatorial Atlantic during the savanna

burning season. Futhermore, *Fishman et al.* [1987] showed that the synoptic distribution of ozone at the surface can strongly influence the distribution of TOMS total ozone during a widespread air pollution episode over the eastern United States. Owing to the nonavailibility of a large number of ozonesonde stations over the world, particularly at tropical regions, *Fishman et al.*, [1990] first attempted to establish the climatological distribution of tropospheric column ozone, referred to as tropospheric ozone residual (TOR), using satellite data (TOMS minus Stratospheric Aerosol and Gas Experiment II (SAGE II) data) between 50°N and 50°S and found a good correlation between the TOR and the total ozone at low latitudes. *Vukovich et al.* [1996] have shown the feasibility of tropospheric ozone residual for nonclimatological studies (daily values, weekly averages, and monthly averages) based on TOMS, SAGE II, and Solar backscattered ultraviolet (SBUV) data and concluded that satellite ozone measurements may be used to infer a qualitative knowledge of the distribution of tropospheric ozone on smaller timescales. To our knowledge, no experimental evidence of ozone transport from stratosphere to troposphere relating to the perturbation of shorter timescales in tropopause structure is reported so far in tropical latitudes.

Though the low latitudinal transport phenomena are different from those of midlatitudes and high latitudes, a special ozone transport campaign was designed to examine it along with the Indian MST radar at Gadanki, near Tirupati (13.5°N, 79.2°E), synchronized with balloon-borne ozonesonde ascents at neighboring station Trivandrum (8.9°N, 76.6°E). The ozonesonde ascent site is about 500-km southward of the radar site. Though the two sites are not colocated, any mesoscale phenomena within a range of 10^3 km can affect both sites simultaneously and to the same degree. The temperature profiles were taken from the routine radiosonde ascents from Madras (13.0°N, 80.0°E), which is about 100 km away from the radar site.

The main thrust of this paper is the quantitative analysis of transport of ozone from stratosphere to troposphere from the ozone vertical profiles following the sudden changes in tropopause structure. In the next section, a description of the Indian MST radar at Gadanki and the Brewer type balloon-borne ozonesonde is presented briefly, and data processing is discussed in detail. In section 3, a brief description is given about the National Center for Medium-Range Weather Forecasting (NCMRWF) general circulation model (GCM) which is used to analyze the large-scale synoptic weather patterns. In section 4 the results of the observations will be discussed in detail. Here we have given a new definition of the sudden changes in tropopause structure. A plausible mechanism, which can qualitatively account for the cause behind these changes in tropopause structure and its effect on the vertical distribution of ozone will be addressed. An effort has been made to examine the role of horizontal advection of ozone due to its spatial gradient in increasing tropospheric ozone, and the geographical distribution of tropospheric ozone residual (TOR) has been analyzed by two data sets obtained independently from Meteor 3 total ozone mapping spectrometers (Meteor 3 TOMS) and the Upper Atmosphere Research Satellite (UARS). Simultaneously, the possibility of horizontal transport of ozone from areas surrounding Tirupati and Trivandrum in enrichment of tropospheric ozone due to synoptic scale circulation has also been verified in detail by close inspection of synoptic weather charts at 1000, 700, 500, and 300 hPa obtained from the NCMRWF GCM at 0000 and 1200 UTC on January 7 and 0000 and 1200 UTC on January 8, 1994. The conclusions will be given in section 6.

2. Experimental Description and Data Analysis

To address the vertical transport during the abnormal behavior of the tropopause, four campaigns were carried out during the period of January 3-8, November 9-16, and December 5-10, 1994 and June 7-24, 1995, using the Indian MST radar at Gadanki (13.5°N, 79.2°E) synchronized with a balloon-borne ozonesonde from Trivandrum (8.9°N, 76.6°E).

With the objective of the determination of tropopause weakening (break), the Indian MST radar was operated in campaign mode. The Indian MST radar is a highly sensitive VHF phased array radar with an operating frequency of 53 MHz and an average power aperture product of 7×10^8 W m^2 [*Rao et al.*, 1995]. The height resolution of radar observation is 150 m. As described by *Jain et al.* [1994], the online data processing carries out fast Fourier transformation (FFT) and incoherent integration of the Doppler spectra. The inclination of the off-zenith beam of radar was taken at an angle of 20°. The 3-dB beam width of the polar diagram is in the range of 2.8°-3°. The experimental specifications are given in Table 1.

The Doppler spectra obtained as output are subjected to the calculation of three low-order spectral moments which provide total signal power, radial wind velocity,

Table 1. Parameter Specifications for Experiments

Parameter	January 1994	November 1994	December 1994	June 1995
Pulse width, μs	16	16	16	16
Wave form[a]	coded	coded	coded	coded
Baud length, μs	1	1	1	1
Height resolution, m	150	150	150	150
Inter pulse period, μs	1000	1000	1000	1000
Beam positions[b]	6	6	6	6
Number of FFT points	128	256	256	256
Number of coherent integrations	128	128	128	128
Number of incoherent integrations	4	1	S (1,2,4)[d]	S (1,2,4)[d]
Output mode of data	spectra	spectra	spectra	Spectra
Doppler resolution, Hz[c]	0.03	0.06	0.06	0.06

[a] Biphase complementary code.
[b] Zenith in EW and NS polarizations, 20 from zenith in zonal and meridoinal planes.
[c] For oblique and vertical beams.
[d] S 1(16:00-21:30 LT), 2(00:00-04:00LT), 4(22:00-00:00, 04:00-06:30).

and its spread for each range bin. The procedure for obtaining these moments is similar to the one for the Poker Flat radar and is briefly described by *Woodman and Guillen* [1974].

The Doppler beam swing (DBS) method as described by *Sato* [1989] is used here in transferring the radial wind vector into three-dimensional wind velocity components U, V, and W, respectively, and the method requires a minimum of three noncoplanar beam positions. Vertical velocity (W component), calculated this way is contaminated by the horizontal wind velocity, which is much greater in magnitude than the vertical wind velocity at each height. It is also obtained independently by using Doppler data from zenith beam alone.

The second moment of the radar signal spectra, i.e., spectral width, yields rms deviation of turbulence. Hence the spectral width can be used to estimate various turbulence parameters. However, the beam width, background horizontal width, and vertical gradient of horizontal winds can contaminate the spectral width [*Hocking*, 1985]. Since 50-MHz radar is very susceptible to specular reflection (especially above the tropopause), the oblique beam spectral width has been used here. The nonturbulent contribution due to beam broadening and shear broadening which depend on the above mentioned factors has been removed from observed spectral width by the method given by *Hocking* [1985].

For the quantitative estimation of ozone transport during and after the tropopause weakening (break), the balloon-borne ozonesonde ascents were taken on radar observation days as given in Table 2. The modified electrochemical Brewer bubbler ozone sensor (Brewer-Mast sonde) (B-M sonde) has been used in the ozonesonde [*Sreedharan*, 1968] for the measurements of ozone profiles. The advantage of modified B-M sonde (Indian sonde) over B-M sonde [*Brewer and Milford*, 1960] is the use of a nonreactive Teflon pump. It is generally flown with standard meteorological radiosondes for measurement of ozone and temperature at different pressure levels. Generally, it ascends up to 30-35 km in the atmosphere.

The ozonesonde sensor consists of an electrotype cell containing a solution of buffered potassium iodide through which ambient ozone-containing air is sucked in by a small pump. The electrodes of the cell are immersed in the solution. The ozone in the air reacts with the KI solution. The reaction results in the liberation of ionic iodine in proportion to the ozone molecules present in the pumped air. This sets up a small current in the electrotype. By applying potential between the electrodes, the current is amplified and transmitted to ground equipment (401-MHz radiotheodilite) for continuous recording of temperature, pressure, and ozone concentration.

Table 2. Campaign Details

MST Radar Operation, Time (Date)	Ozonesonde Operation		
	Time (Date)	Total Ozone, DU	Normalization Factor
	Case 1 (January 3-8, 1994)		
1000 (03-01-94*) to 1800 (03-01-94)	1400 (03-01-94)	230	1.12
1000 (04-01-94) to 1000 (05-01-94)	1000 (04-01-94)	231	0.90
1000 (06-01-94) to 1000 (07-01-94)	1400 (05-01-94)	224	1.11
1800 (07-01-94) to 1800 (08-01-94)	0840 (07-01-94)	233	0.87
	0900 (08-01-94)	223	1.01
	Case 2 (November 9-16, 1994)		
1600 (09-11-94) to 2130 (09-11-94)			
1600 (10-11-94) to 2130 (10-11-94)	2100 (10-11-94)	229	1.12
1600 (14-11-94) to 2130 (14-11-94)			
1600 (15-11-94) to 2130 (15-11-94)			
1600 (16-11-94) to 2130 (16-11-94)	2200 (08-01-94)	234	0.75
	Case 3 (December 5-10, 1994)		
1600 (05-12-94) to 0630 (06-12-94)	2200 (05-12-94)	240	0.61
1600 (06-12-94) to 2130 (06-12-94)	1000 (06-12-94)	240	0.62
1600 (07-12-94) to 0630 (08-12-94)	0900 (08-12-94)	236	1.03
1600 (08-12-94) to 2130 (08-12-94)			
1600 (09-12-94) to 0630 (10-12-94)	1000 (10-12-94)	234	0.60
	Case 4 (June 7-24, 1995)		
1600 (07-06-95) to 0630 (08-06-95)	12:40 (07-06-95)	259	0.90
1600 (12-06-95) to 0630 (13-12-95)	01:30 (13-06-95)	264	1.47
1600 (19-06-95) to 0630 (20-06-95)	01:20 (20:06-95)	246	0.99
1600 (21-06-95) to 0630 (22-06-95)	12:45 (21-06-95)	253	0.87
1600 (23-06-95) to 0630 (24-06-95)	01:50 (22-06-95)	257	0.89
	01:55 (24-06-95)	257	0.89

Times are given in Indian Standard Time.
* Read 03-01-94 as January 3, 1994.

The individual reading taken as units of partial pressure is obtained at various pressure levels from the relation

$$P(\text{micromillibar}) = 4.3\times 10^{-3} \times i \times T \times t \quad (1)$$

where i is the ozone sensor current produced due to the entering of ozone molecules in the external circuit ; T is temperature of the air in degrees Kelvin; and t is the time in seconds for pumping 100 mL of air.

Assuming that the ozone in the atmosphere is present up to 1 hPa, the sonde profile is integrated vertically. The integrated ozone has been normalized by the total ozone measured by Dobson spectrometers at nearby stations. In order to obtain agreement between the integrated sonde profile and the corresponding measured total ozone, some normalization factor has been used to adjust the individual sonde measurements at all altitudes. In the present study, the data quality has been achieved by selecting the normalization factor with a range of 1.3-0.8 ± (0.035-0.1). For ozonesonde data analysis, the volume mixing ratio is used as unit for O_3 concentration. This choice is approximate for investigations of tropospheric O_3, because this quantity is a quasi-conservative property of an air parcel. The O_3, originally measured in micromillibars, have been converted to ppmv by dividing them by the pressure.

The quality of Indian ozonesonde data have been assessed through several intercomparison experiments and found accurate and reliable [*Attmannspacher and Dutch*, 1970, 1981; *Acharya et al.*, 1985a, b; *WMO*, 1994; *Smit et al.*, 1996]. The Indian ozonesonde has recently been intercompared and intercalibrated with ozonesondes in Juelich Ozone Sonde Intercomparison Experiment (JOSIE) [*Smit et al.*, 1996]. The major goal of this intercomparison was to investigate the precision, accuracy, and response of the different ozonesonde types under controlled laboratory conditions as a function of altitude and ozone level. The result of the JOSIE intercomparison shows that the relative deviation of Indian sondes is typically within ± 10-20 %, whereas it was within ±10% with respect to electrochemical concentration cell (ECC) sondes in the third WMO intercomparison in 1991. The precision error is of about ±10-15%. However, the relative precision in the middle stratosphere, where maximum ozone is available, is best. A normalization factor has been used to check the quality of the data.

To verify the role of horizontal advection of ozone due to the spatial gradient in increasing tropospheric ozone, the geographical distribution of tropospheric ozone residual (TOR) has been determined by the analysis of two data sets obtained independently from Meteor 3 total ozone mapping spectrometers (Meteor 3 TOMS) and the Upper Atmosphere Research Satellite (UARS) [*Fishman et al.*, 1990].

Meteor 3 TOMS was launched on Soviet Union's Meteor spacecraft in August 1991 for providing global coverage of the Earth's total ozone by measuring the backscattered Earth radiance in six 1-nm bands (313, 318, 331, 339, 360, and 380 nm). The experiment used a single monochromator and scattering mirror to sample the backscattered solar ultraviolet radiation. Meteor 3 orbit inclined in 82.50^0 precessed relative to the Earth-Sun line with a period of 212 days. Because of the precession of the orbit, the local equator crossing time changed with the same period. The ozone retrieval uses albedo determined as ratio of backscattered Earth radiance to the incident solar irradiance. This required periodic measurements of the solar irradiance. The Meteor 3 TOMS algorithm is identical to the Nimbus 7 TOMS algorithm [*McPeters et al.*, 1996]. For Meteor 3 TOMS total ozone, the absolute error is ±3%, the random error is ±3%, and drift for 40 months is less than ±1%, though somewhat higher at high latitudes. The total ozone measured by Meteor 3 TOMS is in good agreement (within 1%) with the total ozone measured by ground-based Dobson spectrophotometers. The analysis of Meteor 3 ozone data has been discussed in detail by *Herman et al.*[1996]. The version 7 gridded data ($1.0^0 \times 1.25^0$) have been used here. The focus of this study is between 40°E and 120° E in longitude and 0°N and 30°N in latitude.

The ozone profiles measured by the Microwave Limb Sounder (MLS) (versions 3) have been used here for the study of stratospheric ozone and tropospheric ozone residual (TOR). The MLS is aboard the NASA Upper Atmosphere Research satellite (UARS), launched in September 1991, which began measurements of the altitude profiles of stratospheric temperature and composition on October 1, 1991. UARS MLS measurements are obtained from observations of millimeter-wavelength thermal emissions as the instrument field of view (FOV) which is vertically scanned through the atmospheric limb. The measurement latitudinal coverage is from 34 on one side of the equator to 80 on the other. UARS performs a yaw maneuver at ~36-day intervals (a "UARS month"), when MLS high-latitude coverage switches between north and south. Within each UARS month the UARS orbit plane precesses slowly with respect to the Earth-Sun line. The orbit precession causes the measurements to sweep through essentially all local solar times during the course of a UARS month, becoming 20 min earlier each day at a fixed latitude. The UARS orbital motion (7 km/s) during the limb scan smears the profile measurements over ~400 km in a direction perpendicular to the MLS line of sight. The FOV vertical extent at the tangent point for the ozone measurements is ~3 km, the approximate inherent vertical resolution of the measurements. *Waters et al.* [1993] have provided a general description of microwave limb sounding and its features, whereas *Barath et al,* [1993] have described UARS MLS instruments. The validation of UARS MLS ozone measurements is discussed by *Froidevaux et al.* [1996] and *Cunnold et al.* [1996]. Among each of the three MLS radiometers they found that version 3 205-GHz provides more accurate results in the vertical range of 46-0.46 hPa, with 100-hPa retrievals not yet consistently reliable. The precision (rms) of individual ozone measurement is ~0.2 ppmv, with absolute accuracies (~3% to more than 50% for 100 hPa). From these profiles, the amount of ozone in the stratosphere from tropopause (assuming 100 hPa as a reference tropical tropopause) is integrated over a 24-hour period from 0000 to 2400 UT on each day. *Froidevaux et al.* [1994] have compared the zonal mean column ozone of MLS with total ozone of total ozone mapping spectrometer (TOMS). They found that though the spatial

and temporal variations are generally in good agreement, the uncertainties in individual column ozone values from MLS are typically ~7 Dobson units (DU). The integrated ozone has been subtracted from the colocated total ozone amount derived independently from Meteor 3 TOMS on the same day to obtain tropospheric ozone residual (TOR). The details of this procedure are given by *Fishman et al.* [1990]

3. Model Description

The National Center for Medium Range Weather Forecasting (NCMRWF) global circulation model (GCM) which is used to provide first guess fields for the analysis is based on the primitive equations of vorticity, divergence, virtual temperature, log of surface pressure, and specific humidity. These equations include forcing terms, diabatic heating terms, and source/sink terms, which represent physical processes. The model uses the spectral method of horizontal representation of variables and finite difference representation in the vertical, having 18 unequally spaced levels cast on terrim following the sigma coordinate system. The model has higher resolution near the Earth's surface and near the stratosphere. The horizontal resolution of the model is 80 waves in triangular truncation. In Gaussian grid representation, there are 256 grid points in the east-west and 128 in the north-south. This provides roughly 150-km resolution in the horizontal. The model includes most of the important physical processes such as convection, radiation, surface processes, boundary layer processes, and gravity wave drag, etc.

Basically, this model is based on a global spectral statistical interpolation (SSI) scheme. This scheme been adopted from the National Center for Environment Prediction (NCEP) global numerical weather prediction (NWP) scheme [*Parrish and Derber*, 1992]. The SSI scheme is used for preparing objective analyses, which serve as initial conditions for the forecast model. In this scheme, observational residuals (observations of short range, i.e., 6-hour forecasts as first guess at observation location) are analyzed in spectral space. The analysis variables used in the SSI are sigma (P/P_s) level spectral coefficients of the amplitudes of empirical orthogonal functions of vorticity, unbalanced part of divergence, unbalanced part of temperature, unbalanced log of surface pressure, and the mixing ratio. The distinction of balanced and unbalanced variables is a way of implicitly including a linear balance relationship, which is particularly crucial over tropical regions. It is well known that unlike the geostrophic relationship between mass and wind fields which determines the flow over middle and high latitudes, there is no corresponding well-defined relationship over the tropics. The SSI incorporates the mass and wind balance in the analyzed fields by appropriate choice of analysis variables. The details of the scheme are given by *Bansal and Rizvi*[1993].

The NCMRWF GCM is run in operational mode to provide medium-range NWP forecasts from 0000 UTC initial conditions in real time. The model has been extensively used for understanding and prediction of Indian monsoon flow and rainfall. The intercomparrison of the model with other operational global models shows this model to have skill comparable to these models [*Mohanty et al.*, 1994].

4. Results

4.1. Tropopause Detection

The VHF radar at vertical incidence gives rise to strong echoes. These echoes are expected to arise due to Fresnel type reflection/scattering from turbulent irregularities in the radio refractive index. The intensity of turbulent scattering is related to the intensity of turbulence, to moisture levels and moisture gradients, and to the vertical gradient of potential temperature [*Nastrom et al.*, 1989]. Above 10 km the effects of moisture generally become negligible, and the temperature lapse rate below the tropopause becomes nearly adiabatic, leading to less radar returned power. The intensity of turbulence can be parameterized by the loss of aspect sensitivity, Richardson number (Ri) ≤ 0.25 ($0.25 \leq Ri \geq 1.0$ for critical to subcritical layer), wide spectral width, and high vertical gradient of horizontal wind [*Gage and Balsley*, 1980]. It is well known that the lower stratosphere characterized by hydrostatically stable layer leads to high partial specular reflection in addition to turbulent scattering. It results in a sharp increase in returned power just above the tropopause [*Gage and Green*, 1979]. Thus the tropopause is associated with a large positive vertical gradient of signal-to-noise ratio (SNR) [*Gage and Green*, 1979; *Gage et al.*, 1986; *Nastrom et al.*, 1989]. The high returned power due to partial specular reflections just above the tropopause may locate the tropopause qualitatively. However, large positive vertical gradient in SNR can be taken as algorithms of quantitative detection and monitoring of tropopause heights by VHF radar [*Gage et al.*, 1986].

Figure 1a shows a radiosonde temperature profile, taken from nearby radiosonde station Madras on 1730 IST,

January 3, 1994, whereas Figures 1b and 1c represent the corresponding height profile of relative returned echo power and signal-to-noise ratio gradient at vertical incidence of radar, respectively, on 1713 IST, January 3, 1994. The temperature profile (Figure 1a) shows the location of tropopause at ~15-16 km. It coincides with high returned echo power (Figure 1b) and the large positive SNR gradient (Figure 1c) at ~15.5-16 km. High echo power observed at 18 km with equal magnitude at ~15-16 km may also be the location of the tropopause. However, the higher SNR gradient at ~15-16 km than that at 18 km discards this possibility, whereas the large positive gradient of SNR and high returned echo power at ~13-14 km with equal magnitude at ~15-16 km may be the location of the tropopause. The specular reflection dominates over turbulent scattering at the tropopause [*Gage and Green*, 1979]. The loss of aspect sensitivity with respect to zenith angle (Figure 1d), Richardson number (Ri) ≤ 0.25 (Figure 1e), broad spectral width (Figure 1f), and strong vertical gradient of horizontal wind (Figure 1g) at ~13-14 km indicate that turbulent scattering is dominant over partial specular reflection processes. Therefore it can be concluded that the large positive SNR gradient at ~15-16 km can be defined as the location of the tropopause [*Gage et al.*, 1986]. The Richardson number is being calculated from radiosonde temperature profiles taken from nearby station Madras and vertical shear in the horizontal wind of radar observation.

Figure 2a shows that the tropopause in the temperature profiles taken from nearby radiosonde station Madras at 1730 IST on January 7, 1994, and at 0530 IST, January 8,

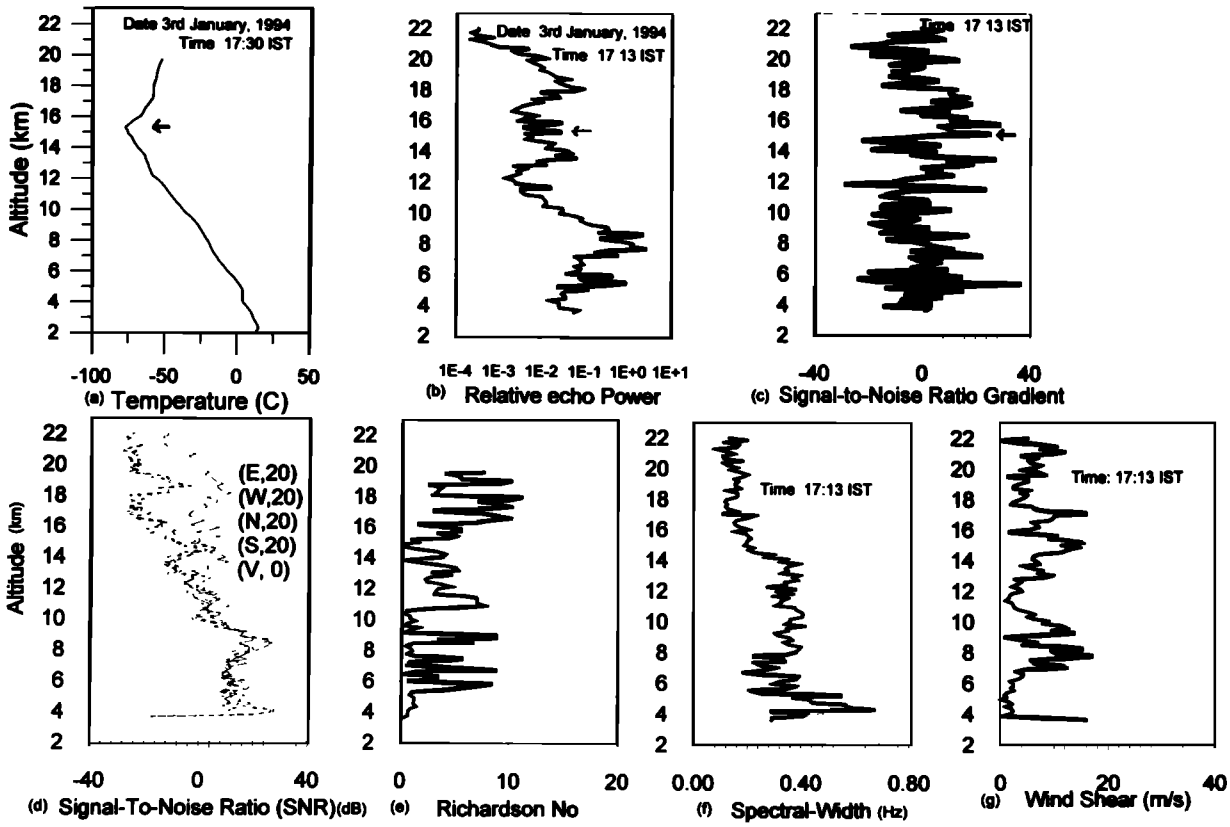

Figure 1. Comparison of the tropopause detected by radar return signal and signal-to-noise ratio (SNR) gradient with the tropopause detected from temperature profile taken from the nearby radiosonde station Madras, for a 'normal' tropopause (100 km away from MST radar). Figure 1a represents the radiosonde temperature profile, Figure1b the corresponding height profiles of radar echo power obtained at vertical incidence, and Figure 1c represents the signal-to-noise ratio gradient. The arrow shows the tropopause measured by the radiosonde at Madras in Figure 1a. Figures 1d, 1e, 1f, and 1g represent the aspect sensitivity, Richardson number, spectral width, and vertical gradient of horizontal wind, respectively.

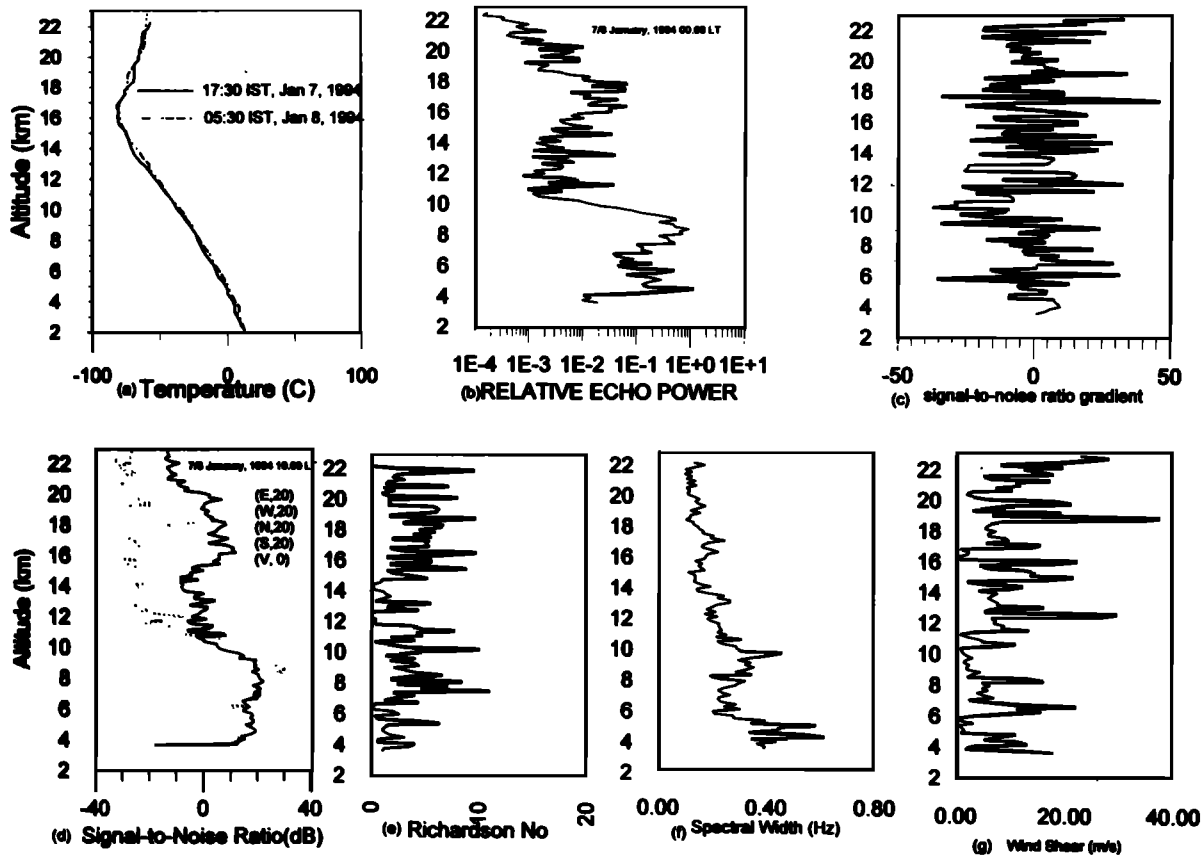

Figure 2. Comparison of the tropopause detected by radar return signal and signal-to-noise ratio gradient observed by vertical incidence of radar with the tropopause detected from temperature profile taken from nearby radiosonde station Madras at tropopause "weakening." Figures 2a-2g represent the same parameters as in Figures 1a-1g but during the tropopause weakening.

1994 is also not well defined according to WMO rules. At 0000 IST on January 8, 1994, the returned echo power at vertical incidence of radar at ~16-18 km (Figure 2b) shows a broad pattern. In addition, it is hard to distinguish the tropopause from other layers by large positive SNR gradient, the physical algorithms of tropopause detection at 0000 IST (Figure 2c). The turbulent parameters, for example, Richardson Number (Ri) near 1 (Figure 2e) and high wind shear (Figure 2g), support the turbulent scattering mechanism near 16-18 km, though the strong aspect sensitivity between 16 and 18 km (Figure 2d) and the presence of narrow spectral width in Figure 2f does not support this hypothesis. However, the analysis of the Figures 2a-2g suggests that it is very difficult to separate the position of tropopause layers from lower and upper stable layers by the Indian MST radar, and it is also reflected in the radiosonde data.

Two points are obvious from the analysis of Figures 1a-1g and Figures 2a-2g. First, the position of the tropopause can be detected by the Indian MST radar aided by radiosonde data. Second, the additional advantage of the MST radar over routinely observed radiosonde data is that it can characterize any modification to tropopause structure. The contour plots of time-height series of real-time observed signal-to-noise ratio gradient may give a comprehensive view of spatial and temporal variations of the layered tropopause, including the stable layers above and below.

4.2. Tropopause Weakening

The sudden changes in tropopause structures are observed several times in the data collected during four

different campaigns. The anomalous structures observed during these four campaigns will be highlighted here.

Figures 3a-3d and 4a-4d represent time-height series of the contour plots of relative echo power and SNR vertical gradient during the period of January 3, January 4-5, January 6-7, and January 7-8, respectively. The signal strength generally decreases with height in the troposphere but increases by about an order of magnitude from the hydrostatically stable regions, mostly due to the specular reflection mechanism. Generally, the lower stratosphere is characterized by large stability returns, and therefore the large relative echo power at 18-20 km suggests that the location of the tropopause may be below 18 km. The large positive gradient in SNR at ~16-18 km on January 3, January 4-5, and January 6-7 quantitatively infers the location of the tropopause. Figure 5 represents the time series of temperature profiles from balloon soundings taken from nearby station Madras. From the Figures 4a-4d and Figure 5 it is obvious that the tropopause defined in temperature profiles at ~16-18 km during January 3, January 4-5, and January 6-7 are coincident with the large positive SNR gradient obtained from the Indian MST radar. However, the location of large vertical SNR gradient during January 7-8 has descended nearly 1 km from the earlier position.

Figures 3b and 4b represent the height-time series of relative echo power and positive signal-to-noise ratio gradient, observed with the vertical incidence of radar from 1023 IST on January 4 to 1000 IST on January 5. The special feature on January 4-5 is that the relative echo power at ~18-20 km and the multiple layered structure at ~17-18 km with large positive gradient in SNR have gradually descended and become indistinguishable from the lower layer at ~13-14 km from 2300 IST on January 4 and retain this structure up to 0100 IST on January 5, 1994. The whole time period of this event is around 3 hours. Unfortunately, no temperature measurement is available during this period, so it is not reflected in the routinely measured temperature profile (Figure 5).

Figures 3d and 4d represent the time-height series of relative echo power and SNR gradient, observed with vertical incidence of radar between 1800 IST on January 7 and 1800 IST on January 8, 1994. On January 7-8, the lower stratosphere characterized by large echo power (at ~17-19 km) suggests that the location of the tropopause may be below 17 km. The large positive SNR gradient near ~15-17 km quantitatively provides the location of the tropopause, reported in the radiosonde temperature profile. Normally, SNR vertical gradient is found at ~16-18 km on other days (January 3, 4-5, 6-7). In addition, another stable layer, which is generally found at ~13-14 km (January 3, 4-5, 6-7) has descended to ~12-13 km. On January 7-8, relative echo power at ~17-19 km, i.e., the lower stratosphere, has disappeared during the periods of 0000-0200 IST and 0900-1000 IST. In addition, the multiple layered structure near the tropopause has suddenly descended and become indistinguishable from the lower stable layers at ~12-13 km, giving the impression that the tropopause has disappeared. Unfortunately, during these particular periods, there was no balloon sounding. Of course, effects have also appeared in the temperature profiles on 1730 IST on January 7 and 0530 IST on January 8. Though the disappearance period of the tropopause is around ~2-3 hours, the total time period of disappearance and regeneration of the tropopause is around ~4-5 hours, which is associated with mesoscale features. Therefore the examination of temperature profiles (Figure 5) during the adjacent period also shows a broad pattern near the tropopause.

Close inspection of the events during January 4-5 and January 7-8, 1994, suggests that the tropopause has become indistinguishable from lower stable layers at ~13-14 km or disappeared for a certain period. It is clear from the relative echo power when it has weakened to negligible. Therefore these events can be termed as "tropopause weakening."

The large positive vertical gradient in SNR has been taken as algorithms of quantitative detection and monitoring of tropopause structure by VHF radar during the period of November 9-16 (Figures 6a-6e) and December 5-10 (Figures 7a-7f), 1994, and June 7-24, 1995 (Figures 8a-8j). The anomalous pattern in tropopause structure, i.e., "tropopause weakening" as seen on January 4-5 and January 7-8, 1994, is also noticed on different shorter timescales during the period of November 9-16 (Figures 6a-6e) and December 5-10 (Figures 7a-7f), 1994, though the tropopause structures show small variations during June 7-24, 1995 (Figures 8a-8j). The anomalous structures observed during these campaigns will be highlighted here.

4.2.1. November 1994. During the second campaign (November 9-16) (Figures 6a-6d) the anomalous structure of the tropopause is observed on November 10 (Figure 6b), November 14 (Figure 6c), and November 16 (Figure 6e). Figure 6b represents the height-time series of positive gradient of SNR observed continuously from 1700 to 2130 IST, November 10, 1994. The large positive SNR

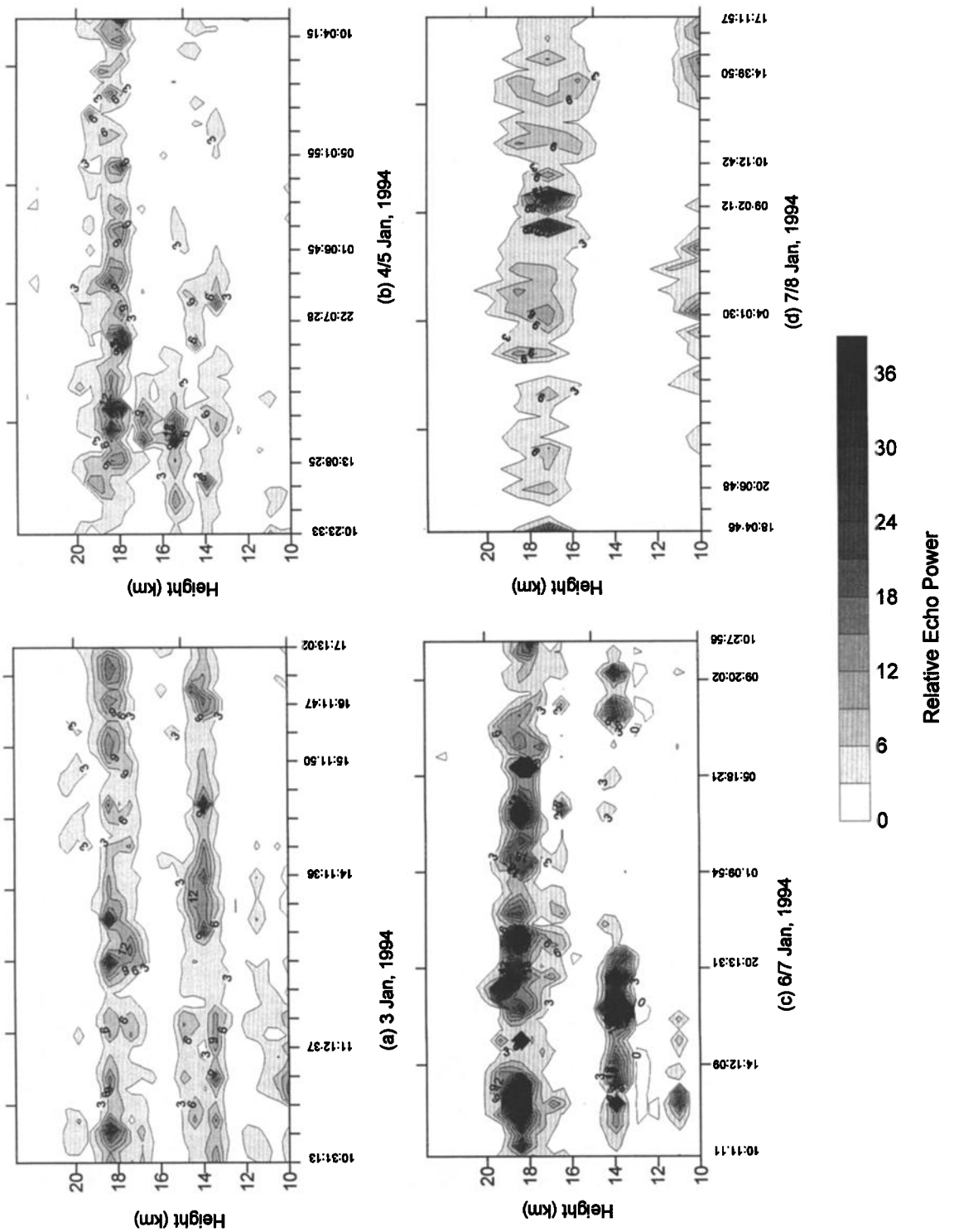

Figure 3. Time series contour maps of echo power observed by the Indian mesosphere-stratosphere-troposphere (MST) radar at vertical incidence during January 3-8, 1994. The time is expressed in Indian Standard Time (IST). The contour interval unit is decibels per 150 m.

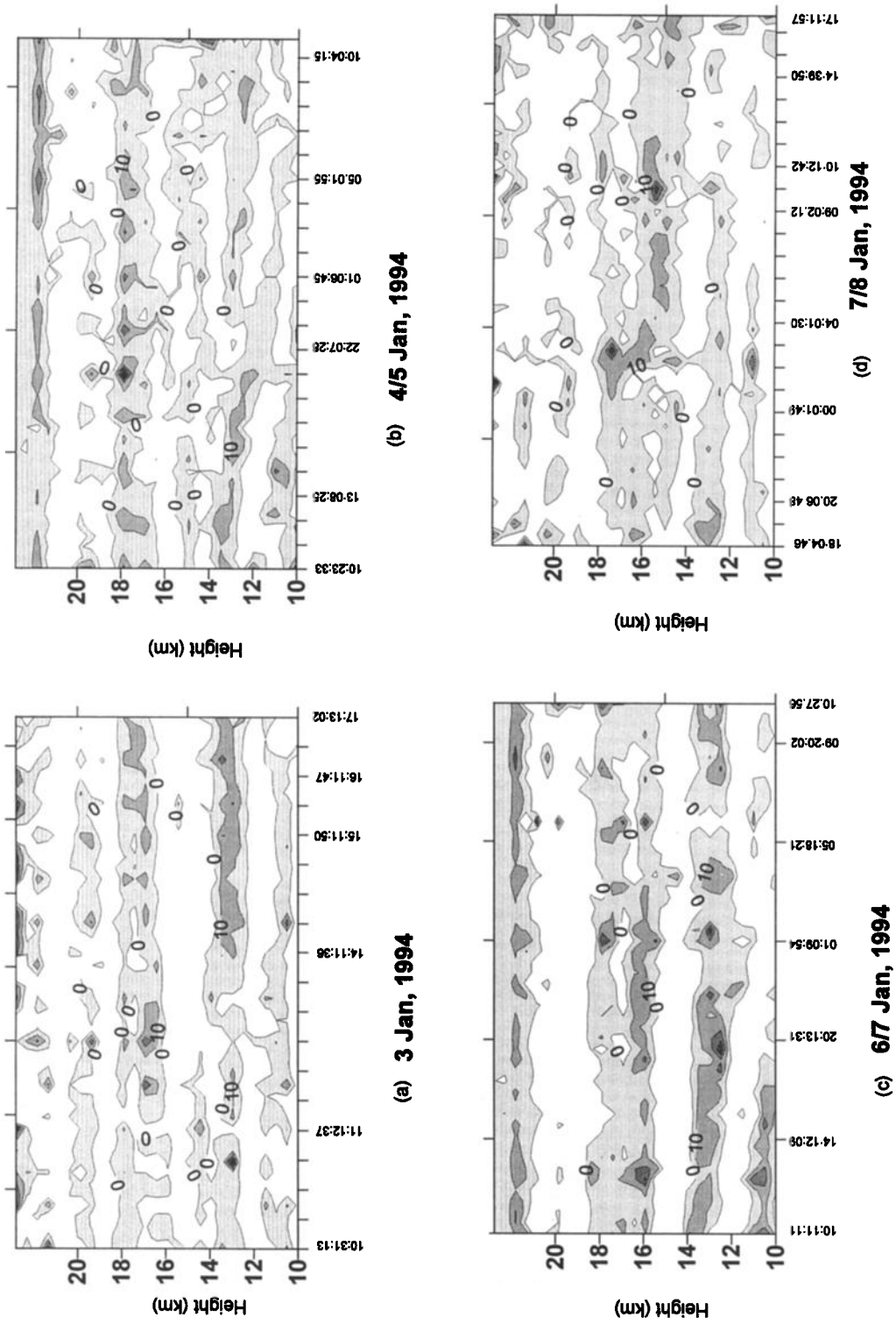

Figure 4. Time series contour maps of signal-to-noise gradient observed by the Indian MST radar at vertical incidence during January 3-8, 1994. The time is expressed in Indian Standard Time (IST). The contour interval unit is decibels per 150 m.

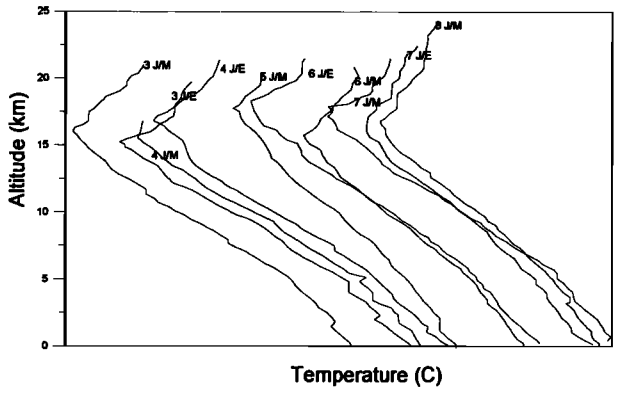

Figure 5. Radiosonde profiles during January 3-8, 1994, taken at nearby radiosonde station Madras.

gradient around 16-18 km represents the location of the tropopause, which is reported in the simultaneous observed rawinsonde temperature profile (not shown). The multiple layered tropopause has suddenly become indistinguishable from the lower stable layer between 1638 IST and 1734 IST. Figure 6c represents the height-time series of positive gradient of SNR observed continuously from 1636 IST to 2130 IST on November 14. The tropopause structures have perturbed for the period of 1720-1930 IST. Similarly, the tropopause structures on November 16, 1994, show an anomalous pattern during the period of 1817-2000 IST (Figure 6e). On November 14 and 16 (Figures 6c and 6e) the tropopause structures have either disappeared or become indistinguishable from lower stable layers, as seen on November 10 (Figure 6b). The time period for the whole process (i.e., disappearance and appearance of the tropopause) is around ~2-3 hours or more, and it may be associated with meso-alpha scale features.

4.2.2. December 1994. During the third campaign (December 5-10, 1994, Figures 7a-7f) the comparative analysis shows the anomalous structure of the tropopause on December 7-8, 1994 (Figures 7c-7d). During December 7-8, 1994, the radar observation is taken from 1600 IST on December 7 to 0630 IST on December 8. The tropopause and the lower stable layers at ~13-14 km have become indistinguishable at 1931 IST on December 7. The pattern remains the same up to 0240 IST, December 8 and regains its shape around 0300 IST, December 8. The tropopause reported in temperature profiles (not shown) taken from radiosonde station Madras on December 7-8 is also not well defined. The morphology in this case is very similar to the other events (i.e., January 4-5, January 7-8, and November 10, 14, and 16).

4.2.3. June 1995. In the above mentioned three campaigns, the sudden changes in tropopause structure are observed on several occasions. The duration of these special features is less than 6 hours or so, which is associated with mesoscale phenomena. However, during the fourth campaign, June 7-24, 1995 (Figures 8a-8j), abnormal behavior of tropopause structure along with height change is not observed as seen during three earlier campaigns (January, November, and December, 1994).

The tropopause structures have been monitored with the Indian MST radar during four campaigns (January, November, and December 1994 and June 1995). The occurrence of tropopause weakening was observed several times in the data collected during the three different campaigns (January, November, and December 1994). The abnormal variability in tropopause structure at midlatitudes is reported by *Nastrom et al.* [1989] by the SNR gradient method with Flatland VHF radar and by *Larsen and Rottger* [1985] by the reflectivity method during frontal passage with sounding system (SOUSY) VHF radar. *Danielson* [1968] has observed that normal ozone concentrations at all levels are affected by stratosphere-troposphere exchange during the abnormal tropopause structure.

4.3. Effect of Tropopause Weakening on Ozone Distribution: Case Studies

The balloon-borne ozonesonde ascents were taken on radar observation days (see Table 2). We have selected some events of tropopause weakening which show the signature of stratosphere-troposphere exchange in ozone profiles. In addition, we have also presented one event of tropopause weakening which does not show exchange of ozone. To verify the effect of tropopause weakening on the ozone concentration, only the main findings will be highlighted here.

4.3.1. Case 1 (January 1994). During the first campaign, i.e., January 3-8, 1994, the radar observations show tropopause weakening on January 4-5 and January 7-8. It has been already discussed in section 4.2. However, the ozonesonde data only on January 8, 1994, show that ozone concentration has been affected at all pressure levels. Therefore the observations made on January 4-5 and January 7-8,1994, have been selected to correlate the effect of tropopause weakening and signature of stratosphere-troposphere exchange of ozone.

Figure 9a shows the ozone profiles measured on 1000 IST, January 4 and 1400 IST, January 5, 1994. The

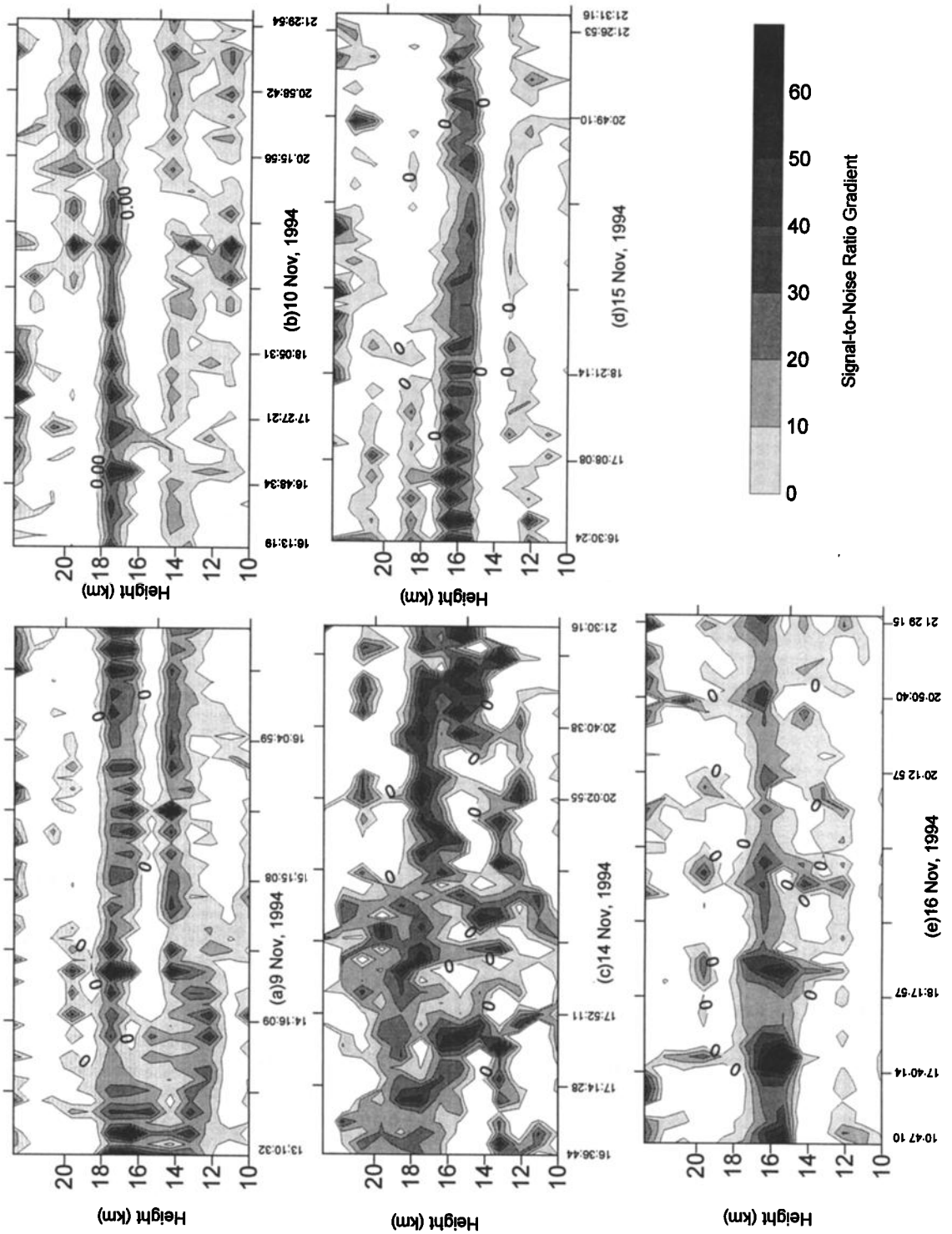

Figure 6. Time series contour maps of signal-to-noise gradient observed by the Indian MST radar at vertical incidence during November 9-16, 1994. The time is expressed in Indian Standard Time (IST). The contour interval is decibels per 150 m.

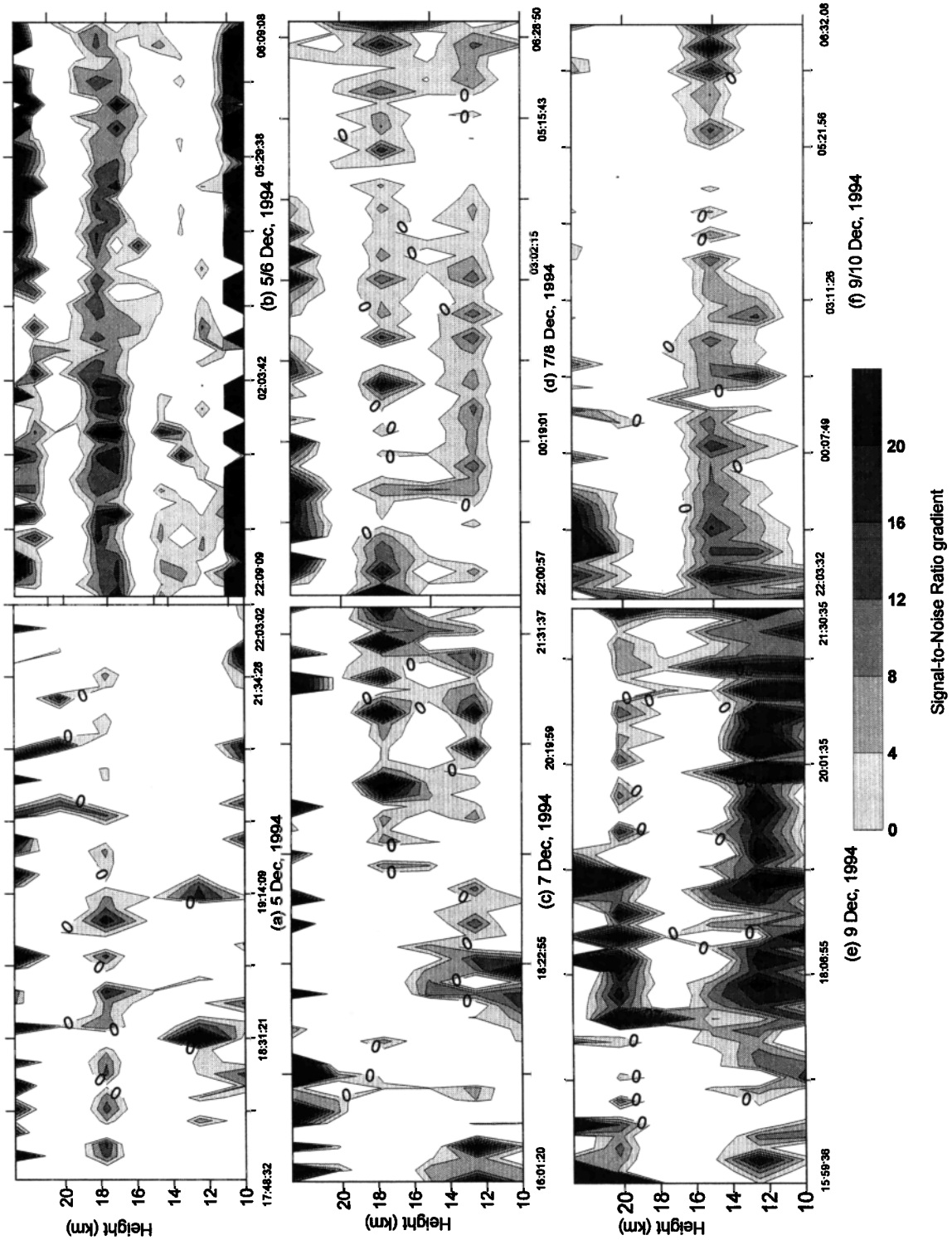

Figure 7. Time series contour maps of signal-to-noise gradient observed by the Indian MST radar at vertical incidence during December 5-10, 1994. The time is expressed in Indian Standard Time (IST). The contour interval unit is decibels per 150 m.

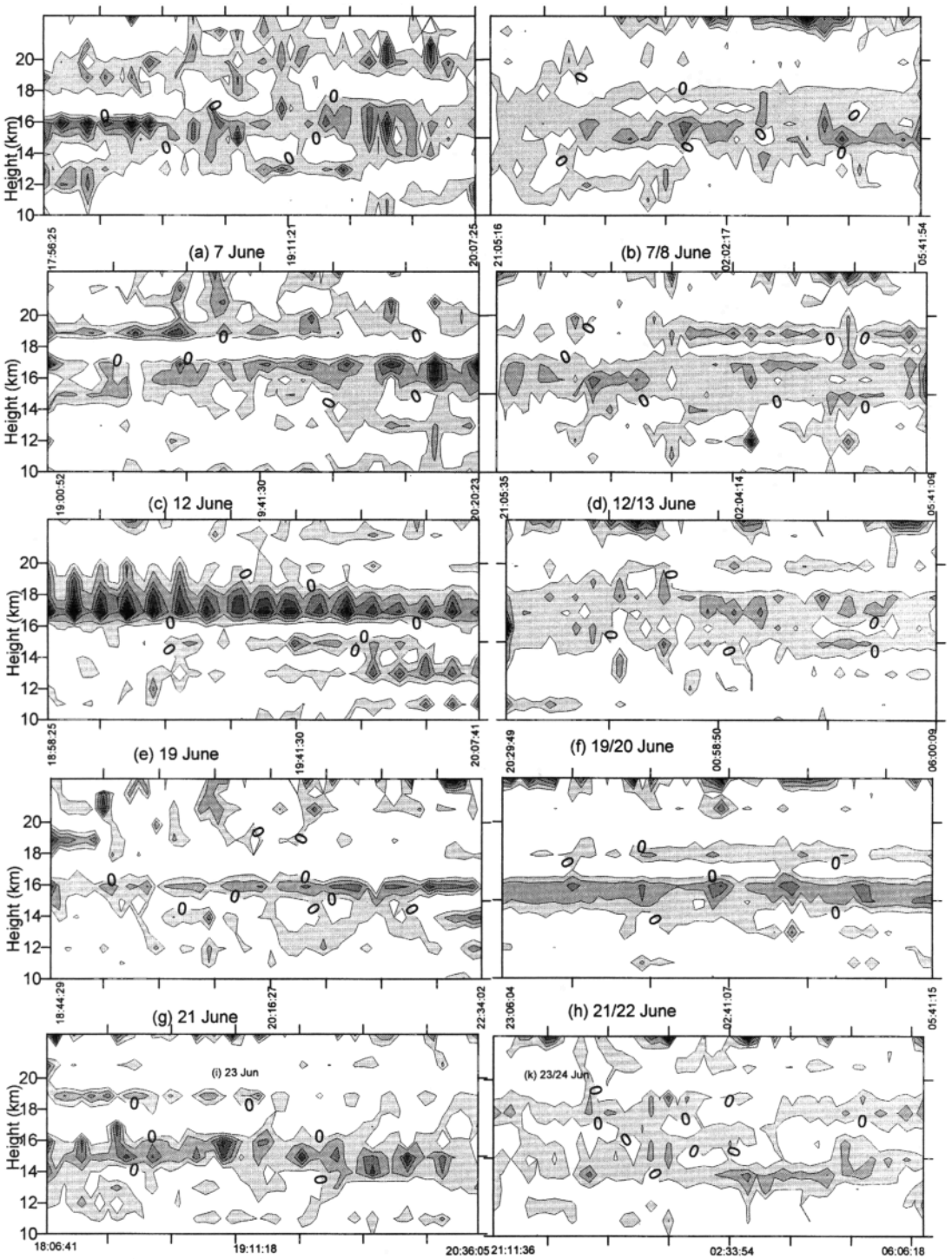

Figure 8. Time series contour maps of signal-to-noise gradient observed by the Indian MST radar at vertical incidence during June 7-24, 1994. The time is expressed in Indian Standard Time (IST). The Signal-to-Noise Ratio gradient which is equal to and greater than zero is plotted here. The contour interval unit is decibels per 150.

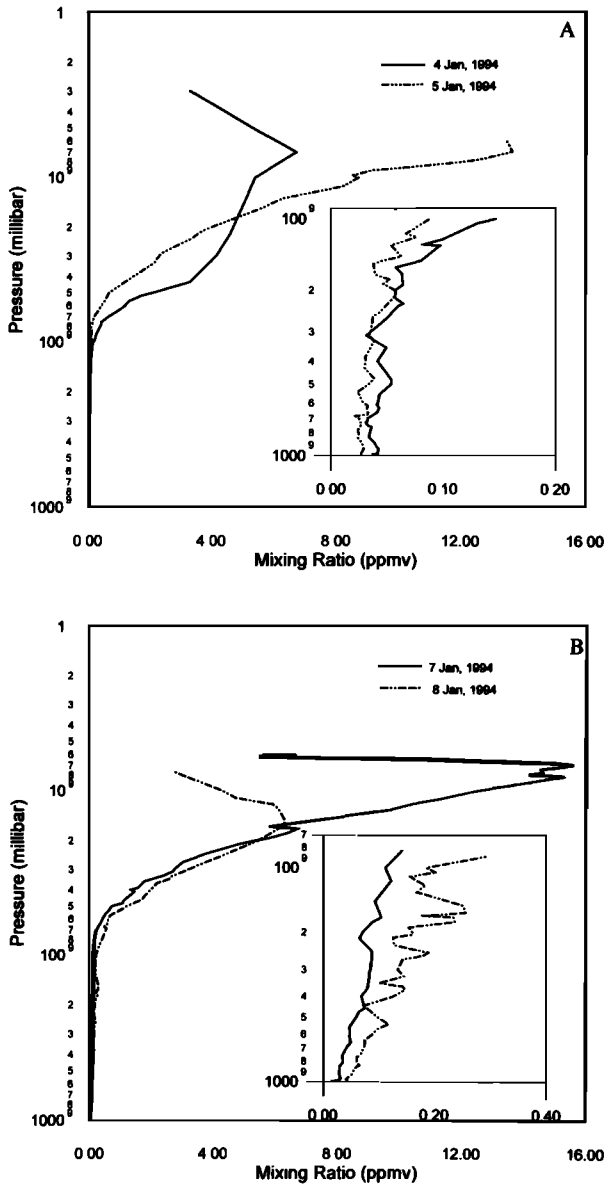

Figure 9. Mixing ratio ozone in ppmv as function of height on radar observation periods (a) January 4-5 and (b) January 7-8. Inset represents the same but up to the tropopause; x axis has been enlarged.

analysis shows that the maximum ozone peak at 8 hPa on January 5 has increased from 6 to 14 ppmv, with a simultaneous decrease in tropospheric ozone concentration from January 4 (Figure 9a). The integrated tropospheric ozone below the tropopause on January 5 has decreased by 11 DU from January 4, though the integrated stratospheric ozone on both days is essentially same. On January 4, only ozone has descended from peak position (~8 hPa) to lower stratosphere (~50 hPa). So there is no evidence of stratospheric intrusion into the troposphere. However, the change in integrated tropospheric ozone may be explained by the same amount of total ozone decrease from January 4 to January 5.

The ozone profiles taken on 0840 IST, January 7, 1994 show that the maximum ozone concentration (~16 ppmv) occurs at around 8~9 hPa (Figure 9b). On January 8, the ozone profile (Figure 9b) taken at 1100 IST shows that the normal peak on January 7, 1994, has come down from ~8-9 hPa to around 20 hPa with peak value (~7 ppmv). Simultaneously, the tropospheric ozone mixing ratio shows a onefold increment, particularly at the upper troposphere (above 200 hPa) where the ozone concentration has increased from 0.10 ppmv on January 7, 1994, to ~0.20-0.30 ppmv on January 8, 1994 (see figure inset where the x axis is enlarged). The integrated ozone from ground to 15 km has increased about 25 DU from the normal value, with the decrease of 30 DU within 25-35 km, where maximum ozone should be available. The total ozone on January 8, 1994, has decreased by nearly 10 DU from the earlier observation (January 6-7). So the discrepancy between the loss in stratospheric ozone and increment in tropospheric ozone is adjusted by the net loss in total ozone from the other days. In

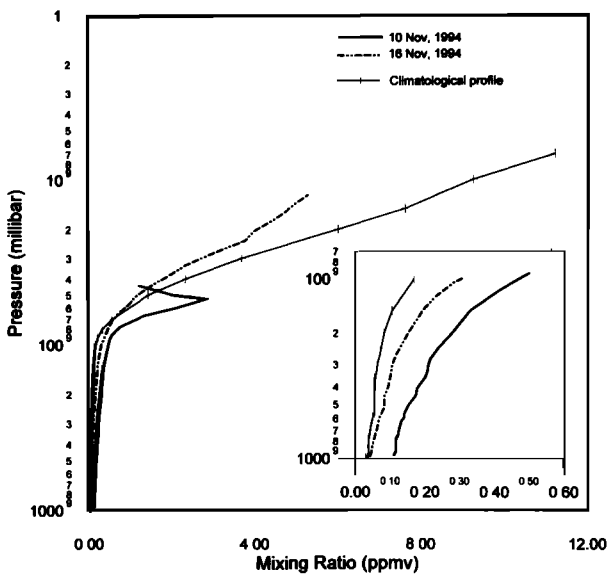

Figure 10. Mixing ratio ozone in ppmv as function of height on radar observation periods November 10 and November 16, 1994. Inset represents the same but up to the tropopause; x axis has been enlarged.

addition, the high ozone concentration at the upper troposphere (above 200 hPa) may not be due to local production of ozone, which generally varies within the range of 0.025-0.050 ppmv.

4.3.2. Case 2 (November 1994). During the second campaign (November 9-16) (Figure 6a-6d) the tropopause weakening is observed on November 10 (Figure 6b), November 14 (Figure 6c), and November 16 (Figure 6e). Unfortunately, there was no ozone measurement during observation on November 14. In addition, no ozone profile is available during normal tropopause structure. Therefore the climatological ozone profile for the month of November, i.e., averaged for that particular months over 26 years (from 1969 to 1994), is used here as normal concentration and compared with the ozonesonde data on November 10 and 16, which show the signature of exchange (Figure 10).

The climatological profile for the month of November shows the stratospheric peak value (~12 ppmv) at 7 hPa. The tropospheric ozone concentration varies from 0.03 to 0.10 ppmv. On November 10, the ozonesonde ascent is taken on 2110 IST, i.e., just after the tropopause weakening (Figure 10). The comparative analysis between the ozone profile on November 10 and the climatological ozone profile shows that the peak value on November 10 has decreased to 3 ppmv with descending of peak height to 60 hPa on November 10. Simultaneously, the tropospheric ozone concentration below 100 hPa which is observed within the range of 0.03-0.10 ppmv shows a 400% increment with maximum value of 0.50 ppmv at the upper troposphere (see figure inset where the x axis is enlarged). On November 16, 1994, the ozonesonde ascent was taken at 2200 IST. The comparative analysis between the ozone profile on November 10 and the climatological ozone profile shows a peak value (~7 ppmv) on November 16 around 20 hPa. The tropospheric ozone concentration on November 16 is observed within the range of 0.05-0.20 ppmv, which is 100 % above of the normal value.

The integrated ozone concentration from ground to tropopause (~100 hPa) that generally varies within the range of 30-40 DU has increased by 30 DU on November 16 and by 50 DU on November 10. This large increment of tropospheric ozone may be compensated for by the same amount of decrease of stratospheric ozone when total ozone remains reasonably same (see Table 2). The normalization factor (equal to 1.12) obtained on the November 10 ozone profile proves the quality of the data.

4.3.3. Case 3 (December 1994). During the third campaign (December 5-10) the ozone profiles on December 8 and 10, 1994, days of tropopause weakening and normal tropopause, respectively, are selected here. The comparative analysis between these two ozone profiles shows the signature of exchange on January 8, 1994. The ozonesonde ascent was taken at 0900 IST on December 8 (Figure 11). On December 8, 1994, the ozonesonde data were available up to 57 hPa. The ozone profiles obtained from MLS within a latitudinal belt of 5.9°N to 17.8°N and a longitudinal belt of 53.3°E to 116.6°E have been averaged on that particular day. The space-averaged 24-hour UARS ozone profile on December 8 has been superimposed on the ozonesonde profile from 68 hPa above. The maximum peak with the magnitude of ~18 ppmv, which normally occurs around 5-7 hPa as seen on December 10, the day of normal tropopause has decreased to 10 ppmv and also come down to 10 hPa on December 8, 1994 (Figure 11). Simultaneously, the ozone concentration (ppmv) below 200 hPa has increased from 0.02 ppmv to ~0.06-0.08 ppmv on December 8 (see figure inset where the x axis is

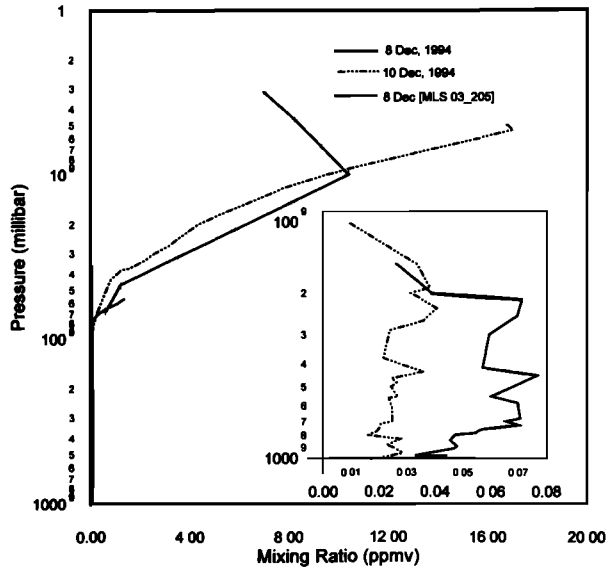

Figure 11. Mixing ratio ozone in ppmv as function of height on radar observation periods December 8 and 10, 1994. On December 8, 1994 the ozonesonde data were available up to 57 hPa. The ozone profiles obtained from Microwave Limb Sounder (MLS) within latitudinal belt of 5.9°N to 17.8°N and longitudinal belt of 53.3°E to 116.6°E have been averaged on that particular day. The space-averaged 24 hours UARS ozone profile on December 8 has been superimposed on the ozonesonde profile from 68 hPa. Inset figure represents the same but up to the tropopause; x axis has been enlarged.

enlarged) through the decrease of stratospheric ozone with a simultaneous increase of tropospheic ozone.

4.3.4. Case 4 (June 1995). In the above mentioned three campaigns, the normal ozone concentration has been occasionally affected by the sudden structural changes in tropopause through the decrease of stratospheric ozone with simultaneous increase in tropospheric ozone. Analysis of the ozonesonde data (Figure 12) during the forth campaign (June 7-24, 1995) shows negligible change in tropospheric ozone concentration (see figure inset where the x axis is enlarged) though there is variation in stratospheric ozone concentration. The variation of upper tropospheric ozone from 0.025 to 0.050 ppmv may be attributed to the relative deviation, which is typically within ±10-20% and the precision error (10-15%) of the instrument. However, this variability in stratospheric ozone can be related to change in total ozone (~18 DU; see Table 2).

5. Discussion

The four campaigns have yielded interesting information on the tropopause weakening of different timescales of different degree. This tropopause weakening may have some effects on the vertical transport of air and chemical tracers. Therefore the discussion can be divided into two modes: the cause of tropopause weakening and its role on chemical tracers transport. For a detail analysis, the observations on January 7-8, 1994 (case 1), will be chosen here.

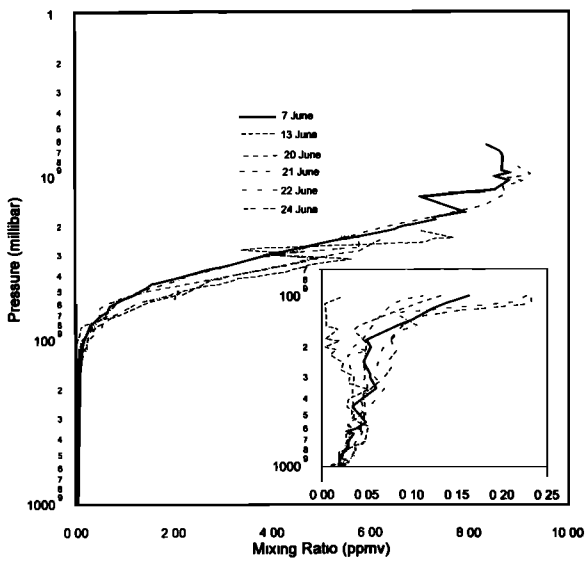

Figure 12. Mixing ratio ozone in ppmv as function of height on radar observation periods June 7, 13, 20, 21, 22, and 24, 1995. Inset figure represents the same but up to the tropopause.

Since the tropopause is a hydrostatically stable region, a large-scale instability in the atmosphere is required to destroy its stability. Earlier research [*Fritts and Rastogi*, 1985] suggests that there is close correspondence between turbulence and/or gravity wave and instability. The detailed study of the effects of gravity wave activity on the tropopause height variation is beyond the scope of this paper. The instability can result in a considerable amount of turbulence throughout the atmosphere [*Fritts and Rostogi*, 1985]. Before the tropopause weakening, the aspect sensitivity and Richardson number (*Ri*) and vertical cross section of horizontal wind, which can measure the role of the intensity of turbulence in weakening the tropopause, will be checked critically.

The aspect sensitivity is an indicator of the inhomogeneity of the structure of scatterers at the scale size of half the radar wavelength [*Waterman et al.*, 1985]. The most commonly used explanation for the less or equal signal-to-noise ratio (SNR) in the vertical direction than in the off-vertical direction is that a turbulent scattering mechanism has dominated over the specular reflection. Figures 13a-13e represent the change in aspect sensitivity during the observation of January 7-8. Equal signal strength at vertical and off-vertical direction above the tropopause at 0000 IST on January 8, 1994, indicates that turbulence has been generated before the disappearance of the tropopause.

Figures 14a-14c represent the instantaneous Richardson number observed before the tropopause weakening (disappearance) on January 7-8. The instantaneous value of the Richardson number is obtained by assuming that the temperature profile is stable over 1 hour. Figures 14a-14c show that most of the 3 to 15-km region is in the subcritical state, which is defined by the Richardson number 0.25-1.0. Of course, the temperature profiles are taken from a radiosonde station which is ~100 km away from the radar site. Instantaneous values of Richardson number often have become quite small and sometimes reach 0.25. The fact that it always takes a positive value seems to suggest that the instability can generate turbulence. It supports the earlier discussion of turbulence generation by instability.

Figure 15a represents the horizontal wind vector (UV plane) on the normal day (January 6-7), whereas Figure 15b represents the horizontal wind vector (UV plane) on January 7-8. Comparison between Figure 15a and Figure 15b suggests that the horizontal wind vector (UV plane)

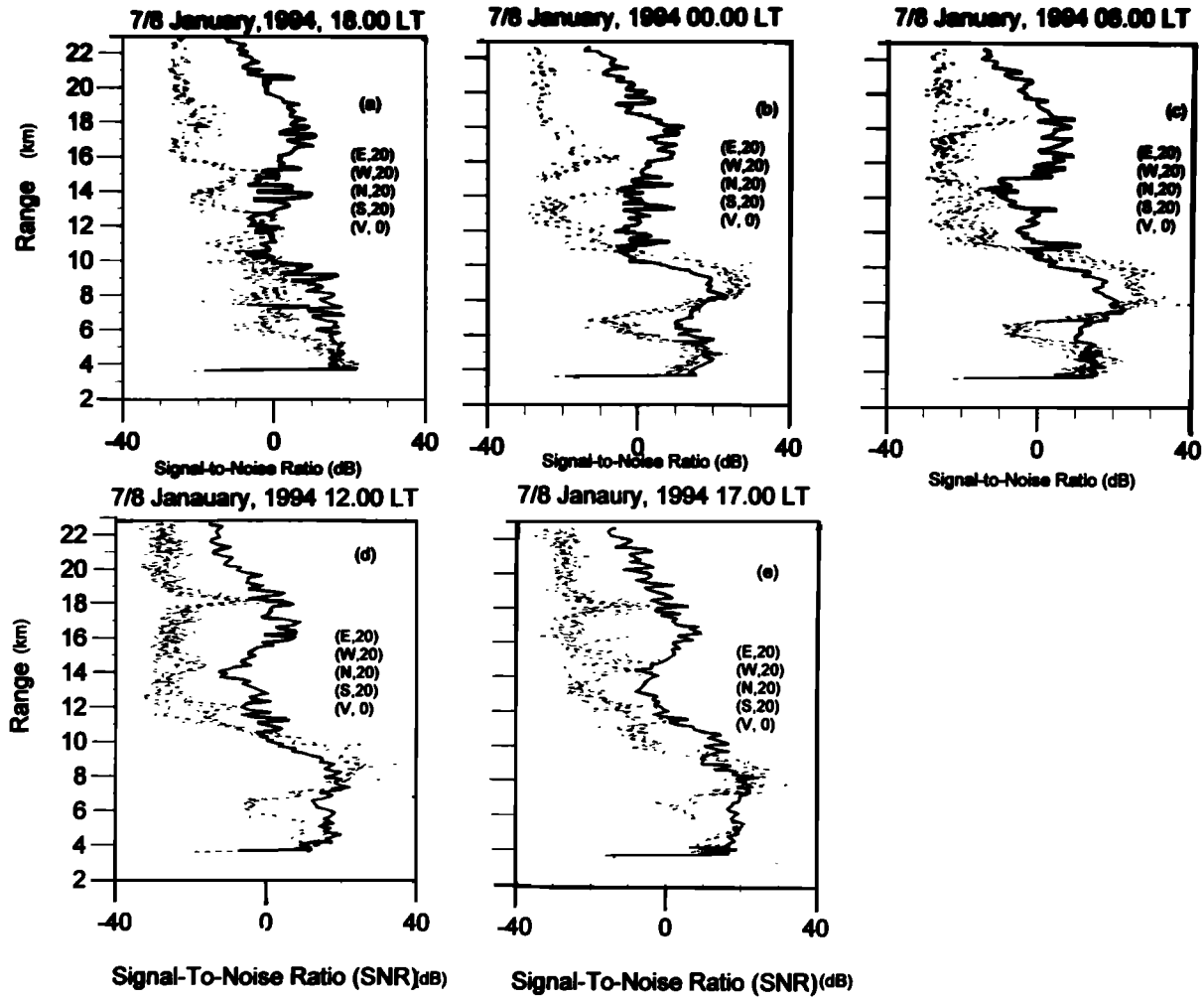

Figure 13. Aspect sensitivity (signal-to-noise ratio for vertical and off-vertical beam of radar) on January 7-8, 1994. Time is mentioned above each panel. Solid curves represent radar return power at vertical beam, and dotted lines represent off-vertical beam.

around the tropopause has become turbulent before the tropopause weakening (disappearance). Thus there is a close correspondence between the turbulent nature of horizontal wind and generation of turbulence. Thus the loss of aspect sensitivity, Richardson number within 0.25-1.0, and turbulent horizontal wind vector (UV plane) all support that the generation of turbulence is the cause of tropopause weakening.

The change in ozone profiles is observed on January 7-8, when tropopause structure has behaved abnormally. Stratospheric ozone is decreased as seen in the ozone profile taken after the weakening of the tropopause (Figure 9b). Simultaneously, the tropospheric ozone concentration shows 100% increment. The integrated ozone (not shown) follows the same patterns when the total ozone remains constant or decreases. This decrease in stratospheric ozone will result from the effects of horizontal advection (divergence) or vertical downward transport or combination of both. The horizontal advection (divergence) will result following the upward displacements (e.g., deep convective events), whereas vertical downward transport is associated with the subsiding motion. However, this vertical downward transport may increase the tropospheric ozone. Of course, the increase in tropospheric ozone may also result from local production or horizontal advection. This horizontal

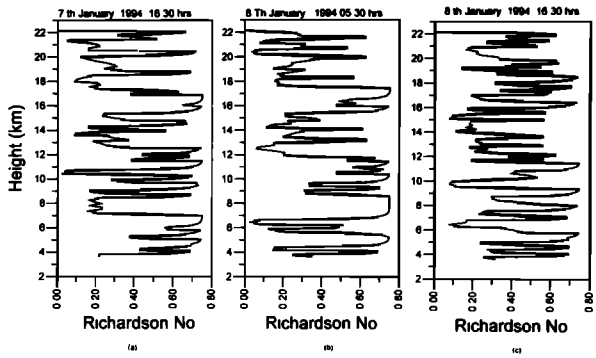

Figure 14. Instantaneous Richardson number at three times on January 7-8, 1994. The Richardson number is calculated with temperature profile taken from nearby station Madras.

advection may result due to its own spatial gradients or with the help of strong horizontal wind from source regions.

The diffused and multilayered tropopause with turbulent wind around the tropopause has generated the possibility of vertical transport. Figures 16a-16d represent the height-time series of vertical wind during the periods of January 3, 4-5, 6-7, and 7-8, respectively. Figure 16b shows the presence of upward velocity during the period of tropopause weakening on January 4-5, and it may not allow mass exchange from stratosphere to troposphere. It is also evident in ozone profiles taken on January 4 and 5, 1994. On January 7-8, during tropopause weakening, the interesting feature is the mixture of downdraft and updraft around the tropopause (Figure 16d). In addition, the magnitude of vertical velocity during the tropopause weakening is low, of the order of few centimeters. Therefore the low order of vertical velocity and/or the mixture of updraft and downdraft might have facilitated the downward vertical mixing between the stratosphere and troposphere and the possibility of horizontal advection of stratospheric ozone due to the upward displacements.

To identify the synoptic features of transport of ozone, the gridded (1.0°×1.25°) total ozone obtained from Meteor 3 has been plotted between 0° and 30°N and between 40° and 120°E in longitude for the period of January 6-9, 1994, keeping the MST radar and Trivandrum as center (Figure 17a-17c). On January 6, it shows that there is a positive latitudinal gradient of 0.50 DU per degree in total ozone from equator to north. However, the magnitude of total ozone at the center for the period January 6 and 7 remains 250 DU, whereas there is a change of 5 DU on January 8, 1994. Though the pattern of changes in total ozone obtained from Meteor 3 TOMS is in good agreement with the measurements of ground-based Dobson spectrophotometer, the changes in column ozone obtained from Meteor 3 TOMS are within the uncertainties in individual column ozone values from Meteor 3 TOMS (absolute error, ±3%, random error, ± 3%).

The integrated stratospheric ozone obtained from MLS has been plotted in Figures 18a-18c for January 6, 7-8, and 8-9, 1994. On January 6, 1994, Figure 17a shows that the absolute value of integrated stratospheric ozone over the region of interest, i.e., Tirupati (13.5°N, 79.2°E) and Trivandrum (8.9°N, 76.6°E), varies within the range of 230-240 DU. In addition, the spatial gradient in the integrated stratospheric ozone from equator to 30°N follows the same variations as total ozone on January 6, 1994. On January 7-8, 1994, the absolute value over the region of interest has decreased by 10 DU. Of course, this decrease is above the uncertainties in individual column ozone value from MLS (~7 DU). On January 8-9, 1994, the region of low integrated stratospheric ozone value has converged around 12°N, 72°E with the absolute value of the order of 215-225 DU. The change in integrated stratospheric ozone on January 7-8, 1994, may be attributed to several factors, for example, the change in tropopause height (100 hPa), which is considered constant here, horizontal divergence, and downward transport. The spatial gradient of integrated stratospheric ozone from the areas surrounding Tirupati and Trivandrum to the region of interest is very negligible, and therefore the decrease in stratospheric ozone may not be the result of horizontal divergence due to its own spatial gradient. In addition, the horizontal displacements may require large upward vertical wind, which was absent on that particular day (Figure 16d). Therefore the decrease in stratospheric may be the result of downward vertical transport, which may increase the tropospheric ozone.

The tropospheric ozone residual (TOR) maps are obtained from Meteor 3 TOMS and integrated column ozone from MLS from 100 hPa (Figure 19a-19c). On January 6, the tropospheric ozone residual (TOR) over the region of interest is of the order of 10-15 DU. The possibility of enrichment of tropospheric ozone at the site of interest (Tirupati and Trivandrum) due to horizontal advection because of its own spatial gradient is possible only from three regions centered at 30°N, 65°E; 30°N, 95°E; and 15°N, 45°E. On January 7-8, the magnitude of TOR has increased by 10 DU over the same region from

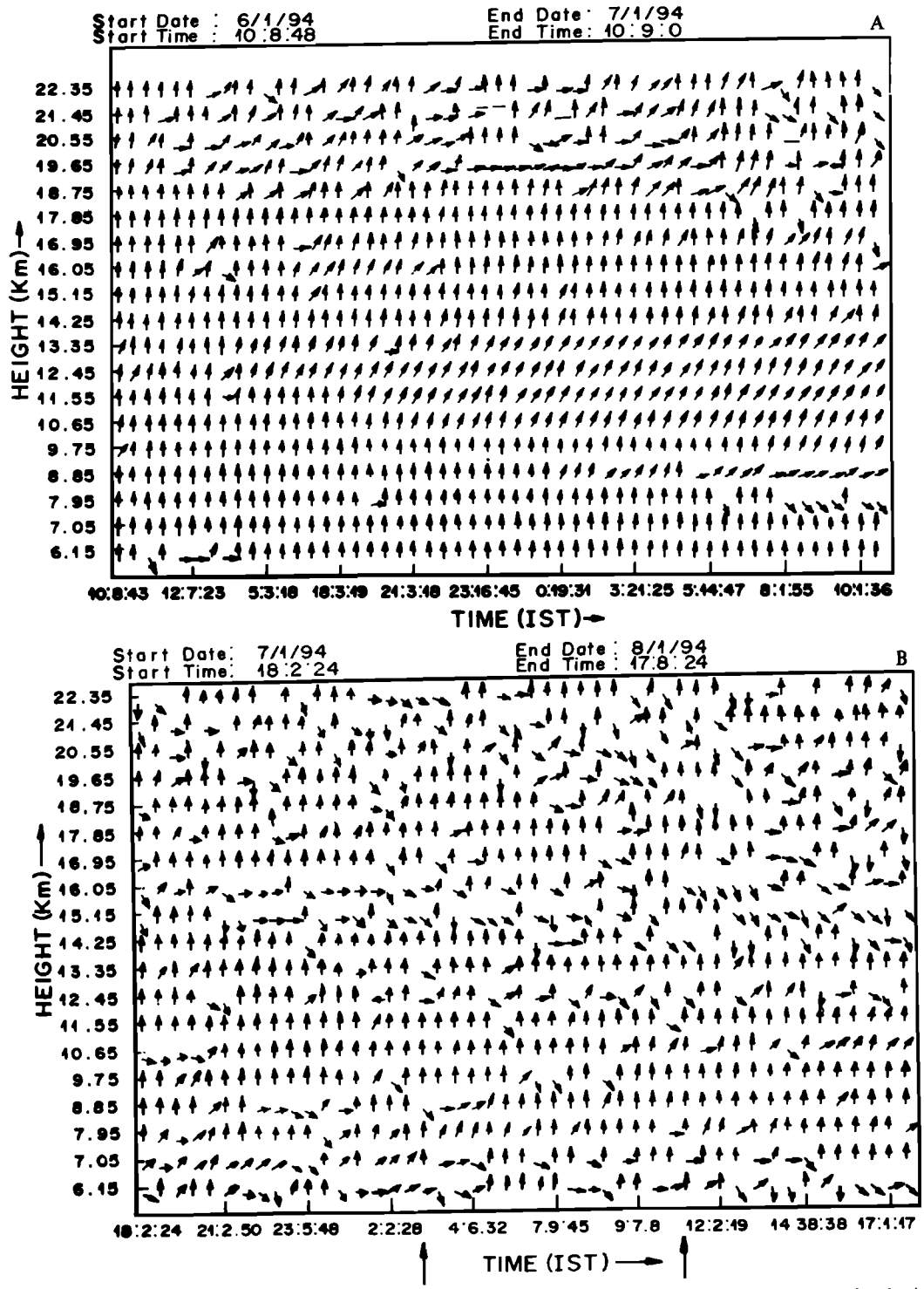

Figure 15. The angle between zonal and meridional velocity is taken as a direction of horizontal velocity. The change in direction is plotted as a function of height and time. U and V are plotted along the Y and X axes, respectively. Generally, positive values of U and V represent the eastward and northward direction of zonal and meridoinal velocity respectively. Figure 15a. is the direction of horizontal velocity on January 6-7, 1994 (normal day). Figure 15b. is the direction of horizontal velocity on January 7-8, 1994. The arrows indicate the period of tropopause weakening. The magnitude of horizontal wind vector is chosen as an arbitrary unit.

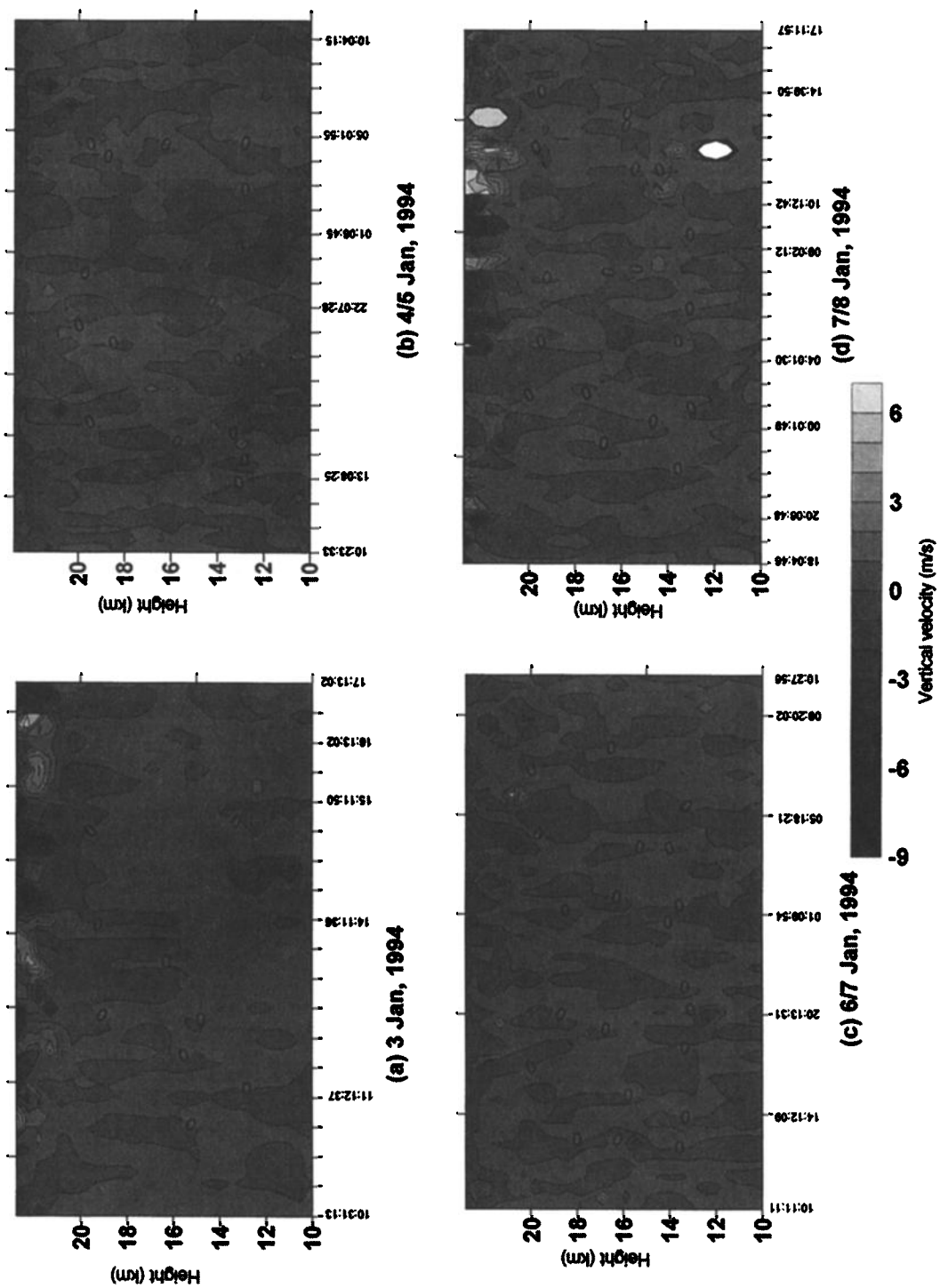

Figure 16. Time series of vertical velocity contour maps, taken from vertical beam observation of radar, are plotted here as a function of height and time. The magnitude of vertical velocity in m/s is given in the figures.

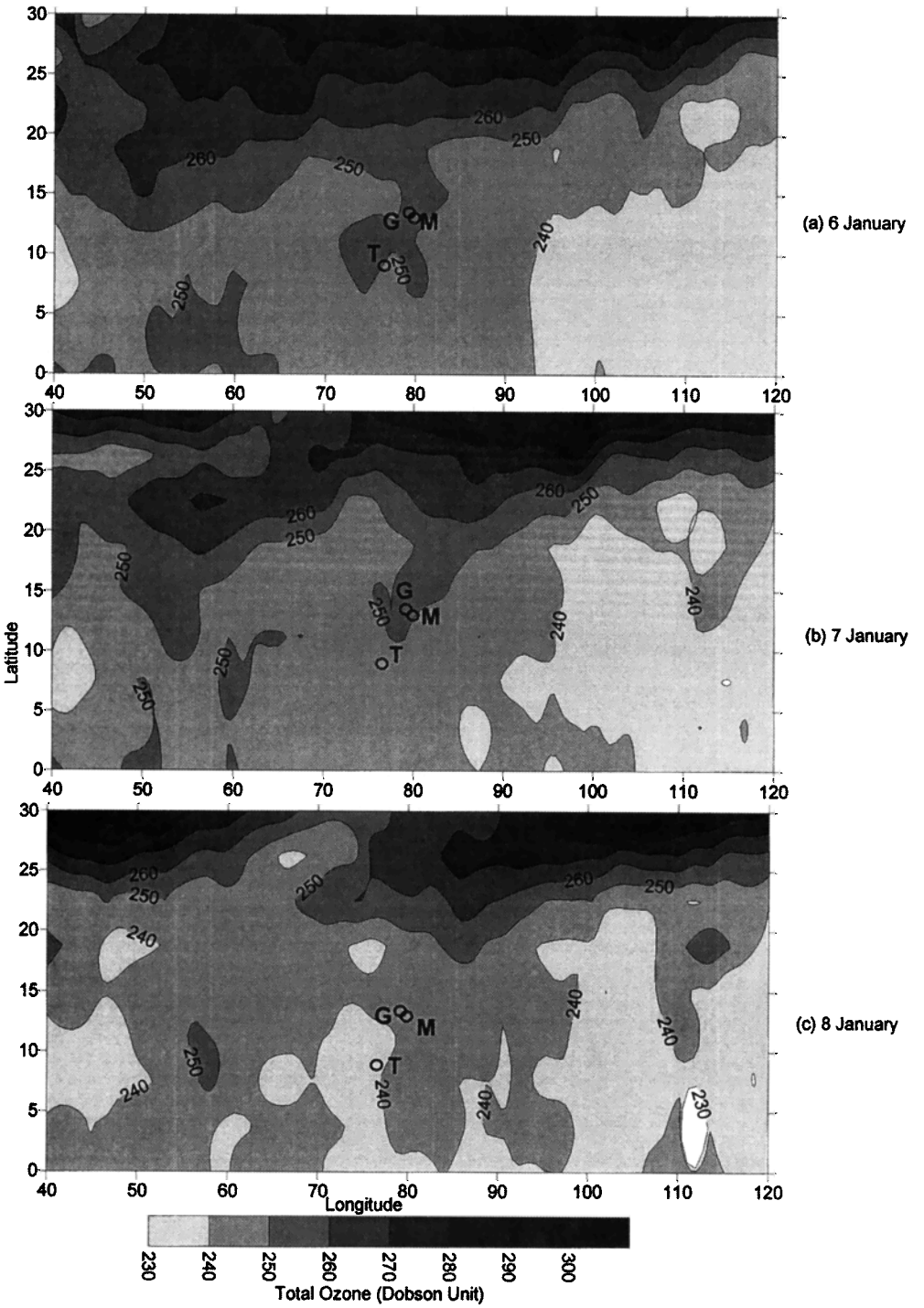

Figure 17. Contour maps of total ozone obtained from Meteor 3 total ozone mapping spectrometers (TOMS) satellite during January 6-8, 1994, within the latitudinal belts of 0°-30^{0}N and longitudinal belts of 40°-120^{0}E. M stands for Madras (radiosonde site), G stands for Gadanki (MST radar site), and T stands for Trivandrum (ozonesonde ascents site).

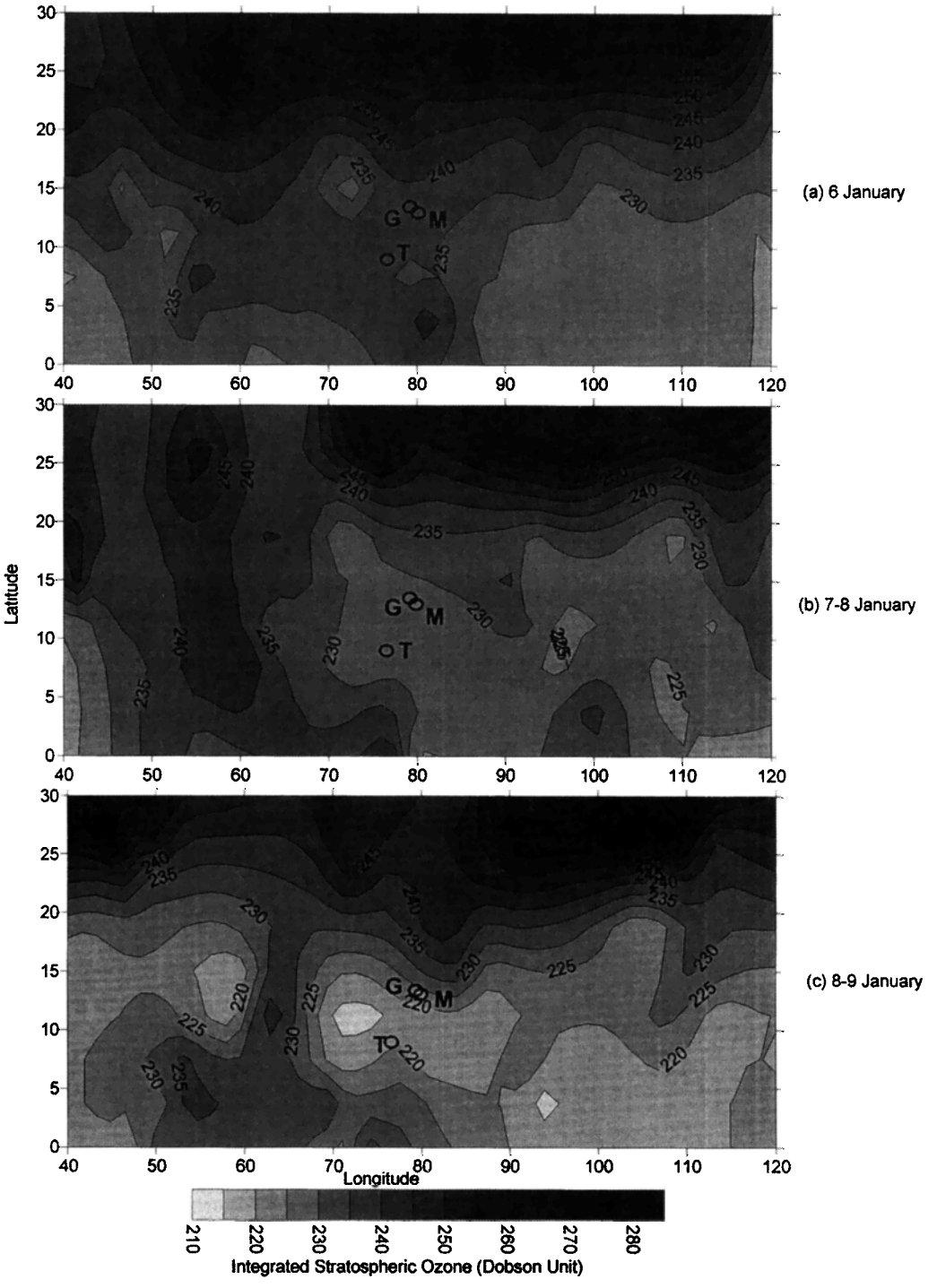

Figure 18. Contour maps of integrated stratospheric ozone (from 100 hPa above) obtained from Microwave Limb Sounders (MLS) on board the NASA Upper Air Research Satellite (UARS) during January 6-9, 1994, within the latitudinal belts of 0°-30^{0}N and longitudinal belts of 40°-120^{0}E. M stands for Madras (radiosonde site), G stands for Gadanki (MST radar site), and T stands for Trivandrum (ozonesonde ascents site).

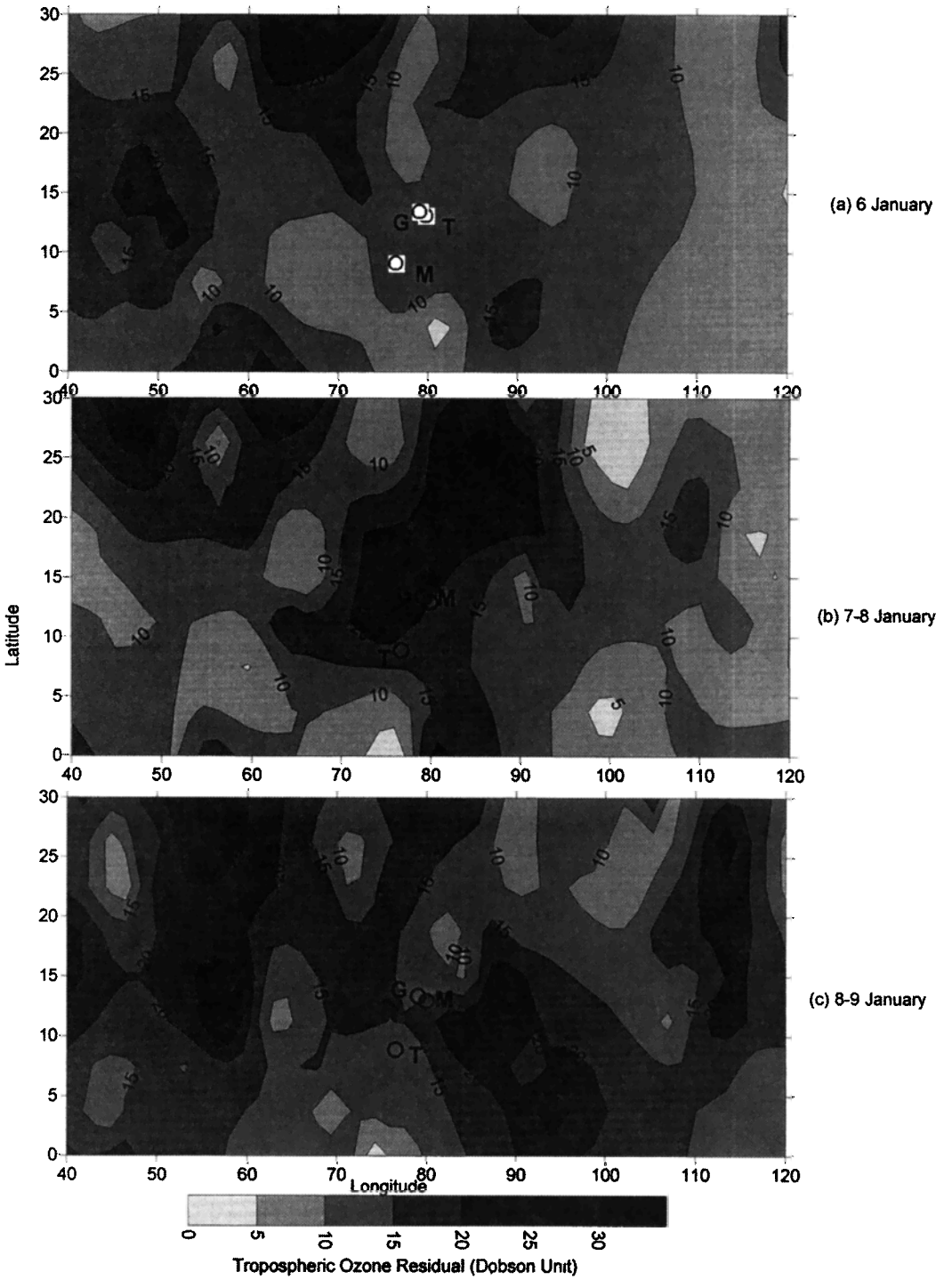

Figure 19. Contour maps of residual tropospheric ozone (obtained by subtracting the integrated stratospheric ozone from 100 hPa above obtained from Microwave Limb Sounders on board UARS from total ozone obtained from Meteor 3 TOMS satellite during January 6-9, 1994, within the latitudinal belts of 0°-30^{0}N and longitudinal belts of 40°-120°E. M stands for Madras (radiosonde site), G stands for Gadanki (MST radar site), and T stands for Trivandrum (ozonesonde ascents site).

the earlier day, with a large absolute value of 25 DU at 25°N, 85°E. On January 8-9, 1994, the absolute value over the region of interest almost remains the same. However, the increase of TOR on January 7-8, 1994, is above the uncertainty of time dependent tropospheric change of Meteor 3 TOMS (0.05per percentage change) and may be attributed to two factors: horizontal advection and downward transport. To explain the sudden increase of TOR by horizontal advection, a very large spatial gradient or large horizontal wind or combination of both is required. However, the sudden increase of TOR may not be explained only by the horizontal advection due to negligible spatial gradient in TOR.

The analysis of synoptic weather patterns between 0^0-20^0N and 60^0-90^0E before and after the perturbed structure of the tropopause may reveal the possibility of horizontal transport of ozone from areas surrounding Tirupati (13.5°N, 79.2°E) and Trivandrum (8.9°N, 76.6°E) in enrichment of tropospheric ozone concentration. For diagnostics purposes, NCMRWF analysis of routine upper air observations at 1000, 700, 500, and 300 hPa at 0000 UTC (0530 IST) and 1200 UTC (1730 IST) are used here. The perturbed structure of the tropopause is observed during the period of 1831-2231 UTC, January 7, 1994, and 0332-0442 UTC, January 8, 1994. The ozonesonde ascents were taken on 0840 IST, January 7 and on 1100 IST, January 8, 1994. The analysis at 0000 UTC, January 7, 1994, is used to define previous conditions, while the analysis at 1200 UTC, January 7, 1994, and 0000 UTC, January 8, 1994,

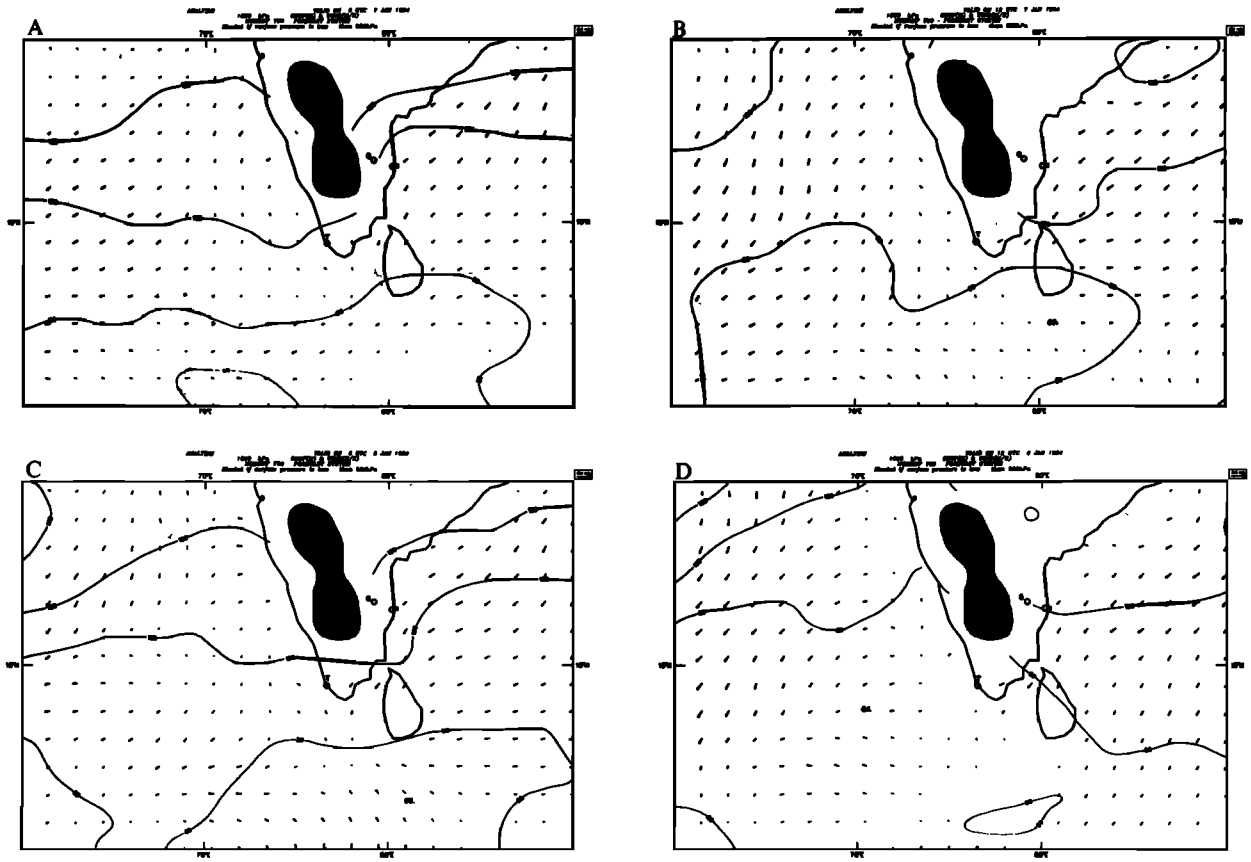

Figure 20. The synoptic scale horizontal wind and geopotential analysis given by the National Center for Medium-Range Forecasting general circulation model (T80) at 1000 hPa (a and b) for 0000 and 1200 UTC on January 7, 1994, and (c and d) 0000 and 1200 UTC on January 8, 1994. The contour interval of geopotential height is 20 m. The magnitude of horizontal wind is 20 m/s, given above the figure as a unit. M stands for Madras (radiosonde site), G stands for Gadanki (MST radar site), and T stands for Trivandrum (Ozonesonde ascents site).

is used to interpret more directly; 1200 UTC, January 8, 1994, is used to define large-scale synoptic weather pattern during the regained normal tropopause structure.

The visual inspection of weather charts at 1000 hPa at 0000 UTC, January 7, 1994 (Figure 20a), suggests that the quasi-meridional flow (i.e., southwestward) in the latitudinal belts of 10^0-20^0N has changed its direction and become zonal (westward) in the latitudinal belts of 0^0-10^0N. The quasi-meridional flow within the latitudinal belts of 10^0-20^0N which was observed at 0000 UTC has become meridional (southward) within the region of 60^0-70^0 E with a small increment of wind speed at 1200 UTC, January 7, 1994 (Figure 20b). However, during the period of 0000-1200 UTC, January 8, 1994 (figures 20c and 20d), the flow has gained the wind pattern of 0000 UTC, January 7, 1994. The comparative analysis of the weather charts at 1000 hPa during the period of 0000 UTC, January 7, 1994, to 1200 UTC, January 8, 1994, shows no sudden changes in the geopotential heights as well as wind pattern.

The analysis of the weather chart at 700 hPa on 0000 UTC, January 7, 1994 (Figure 21a), shows that the zonal flow (westward) which is observed within latitudinal belts of 0^0-5^0N has turned into quasi-meridional (northwestward) within the region of 60^0-75^0E after 5^0N. At 1200 UTC, January 7, 1994 (Figure 21b), the zonal flow pattern (westward) has expanded up to 10^0N, but after 10^0N the wind speed has decreased though the flow pattern is the same as earlier. At 0000 UTC, January 8, 1994 (Figure 21c), a quasi-zonal flow (i.e., westward) is observed within the region of 0^0-10^0N, but within the latitudinal belts of 10^0-20^0N the quasi-meridoinal flow which is observed at 0000 UTC, January 8 has suddenly become meridoinal within the region of 60^0-65^0E, though the wind speed is about 1 m/s. However, at 1200 UTC, January 8, 1994 (Figure 21d), the flow pattern follows the same pattern of 1200 UTC, January 7, 1994.

Weather chart analysis at 500 hPa at 0000 UTC, January 7, 1994 (Figure 22a), shows that flow pattern is zonal (westward) within the latitudinal belt of 0^0-5^0N, but

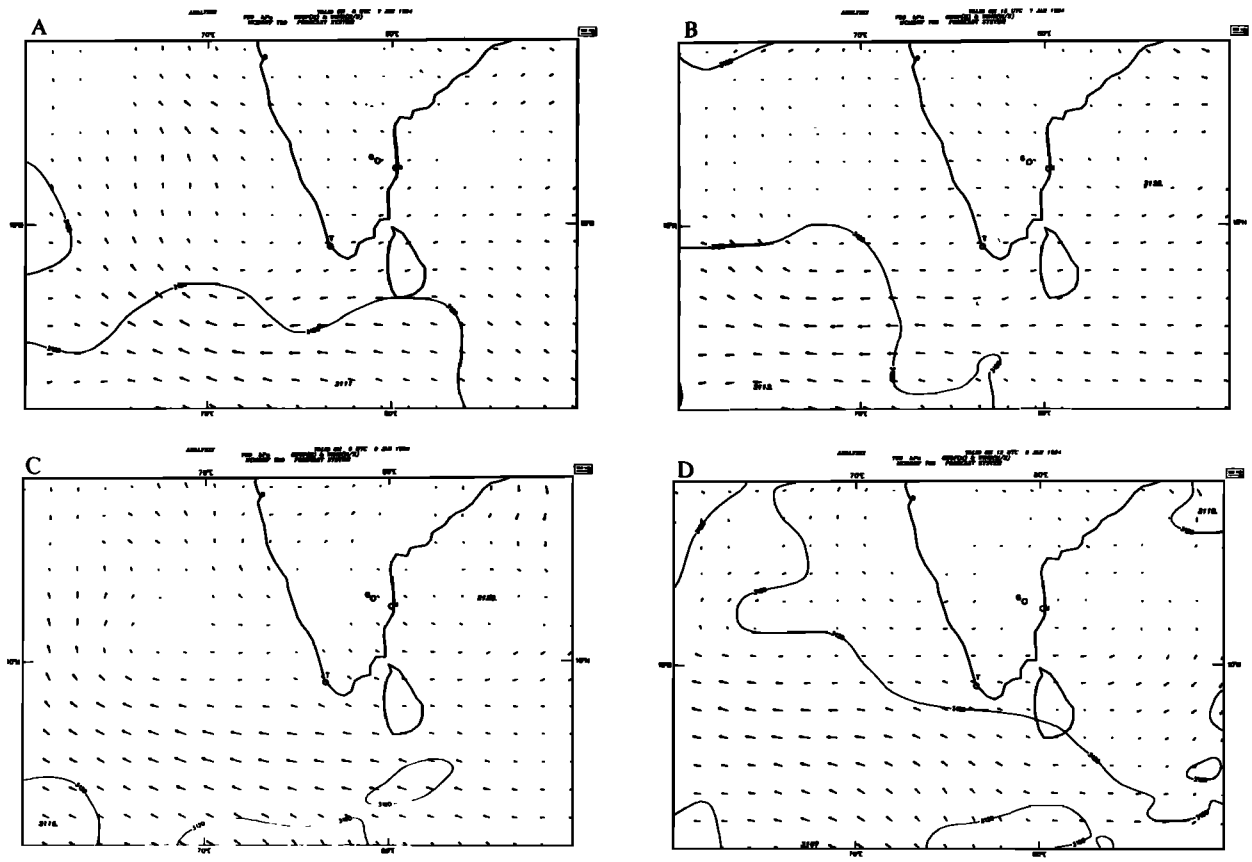

Figure 21. The same as the Figure 20 but at 700 hPa.

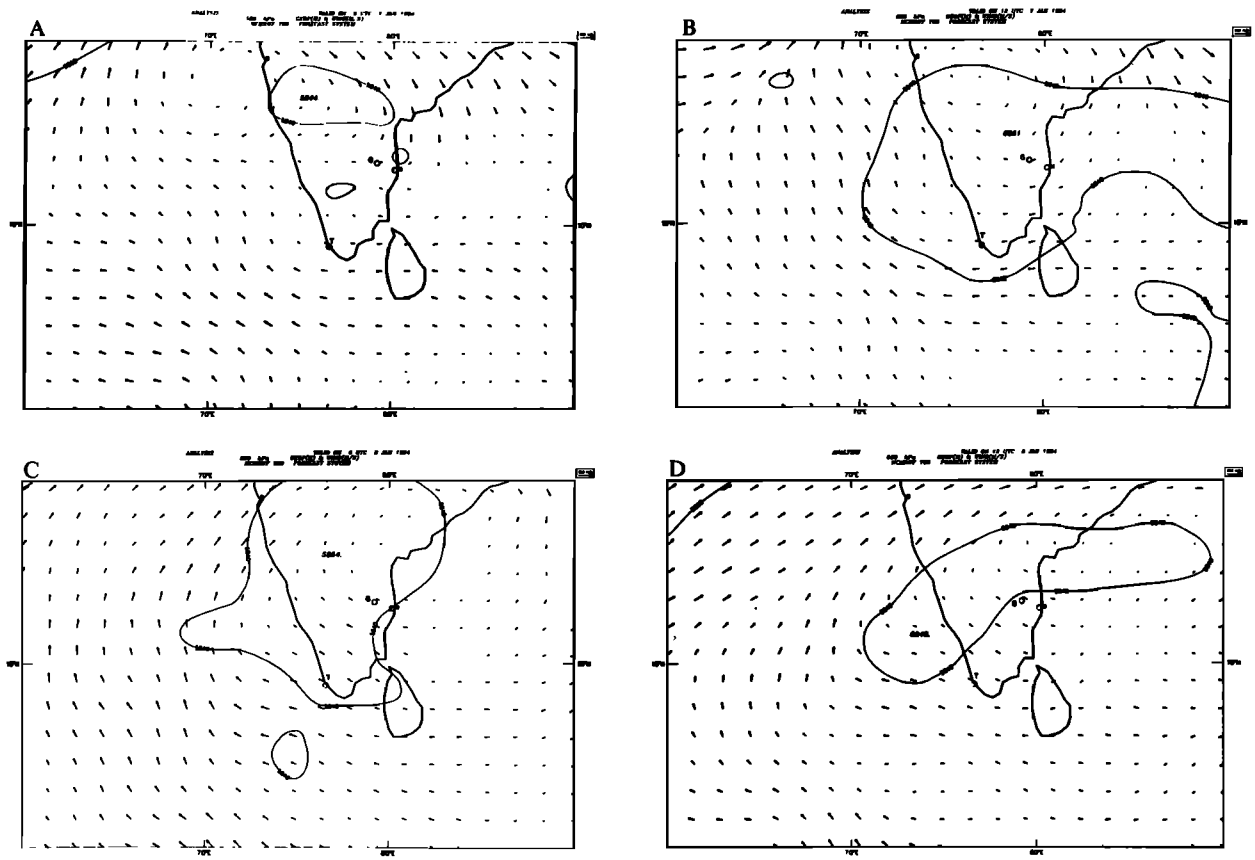

Figure 22. The same as the Figure 20 but at 500 hPa.

after 5°N, flow has suddenly turned toward the northwest direction, making a small vortex around 15°N, 70°E within the region of 15°N, 70° E to 15° N, 90° E. At 1200 UTC, January 7, 1994 (Figure 22b), the flow pattern remains almost the same as observed at 0000 UTC, January 7, 1994, except the center of the vortex is shifted from 70°E to 80°E. However, at 0000 UTC, January 8, 1994 (Figure 22c), the region of the trough has expanded with small eastward displacement of center. At 1200 UTC, January 8, 1994 (Figure 22d), a large cross-contour flow is observed (i.e., the so-called ageostropic flow) in the latitudinal belt of 10° -20°N, with more eastward displacement of the trough region.

The visual inspection of weather chart at 300 hPa during the period of 0000-1200 UTC, January 7, 1994 (Figures 23a and 23b), suggests that a large quasi-zonal flow (northeastward) is observed within the latitudinal belts of 10°-20°N. However, during the period of 0000-1200 UTC, January 8, 1994 (Figures 23c and 23d), a small vortex is formed around the position of 10°N, 80°E with large quasi-zonal flow (northeastward) in the latitudinal belt of 10°-20°N.

Three points are clear from the analysis of synoptic weather charts at 1000, 700, 500, and 300 hPa during the period of 0000 UTC, January 7, 1994, to 1200 UTC, January 8, 1994 (Figures 20-23). First, there is no sudden change in wind pattern and its magnitude, which is generally observed with midlatitudinal tropopause folding/break. Second, the large spatial difference in geopotential height contour of 20-m intervals shows that the same thermal structure is prevailing over Tirupati and Trivandrum during the period of 0000 UTC, January 7 to 1200 UTC, January 8, 1994. Third, the wind direction at 300 hPa has changed to northeastward from westward at lower levels (1000, 700, and 500 hPa) to northward. The northward horizontal wind vector (UV plane) in Figures 15a and 15b observed by MST radar is consistent with synoptic weather patterns. The sudden changes in tropopause structures and wind vector direction observed by radar on timescales less than a few hours or so are

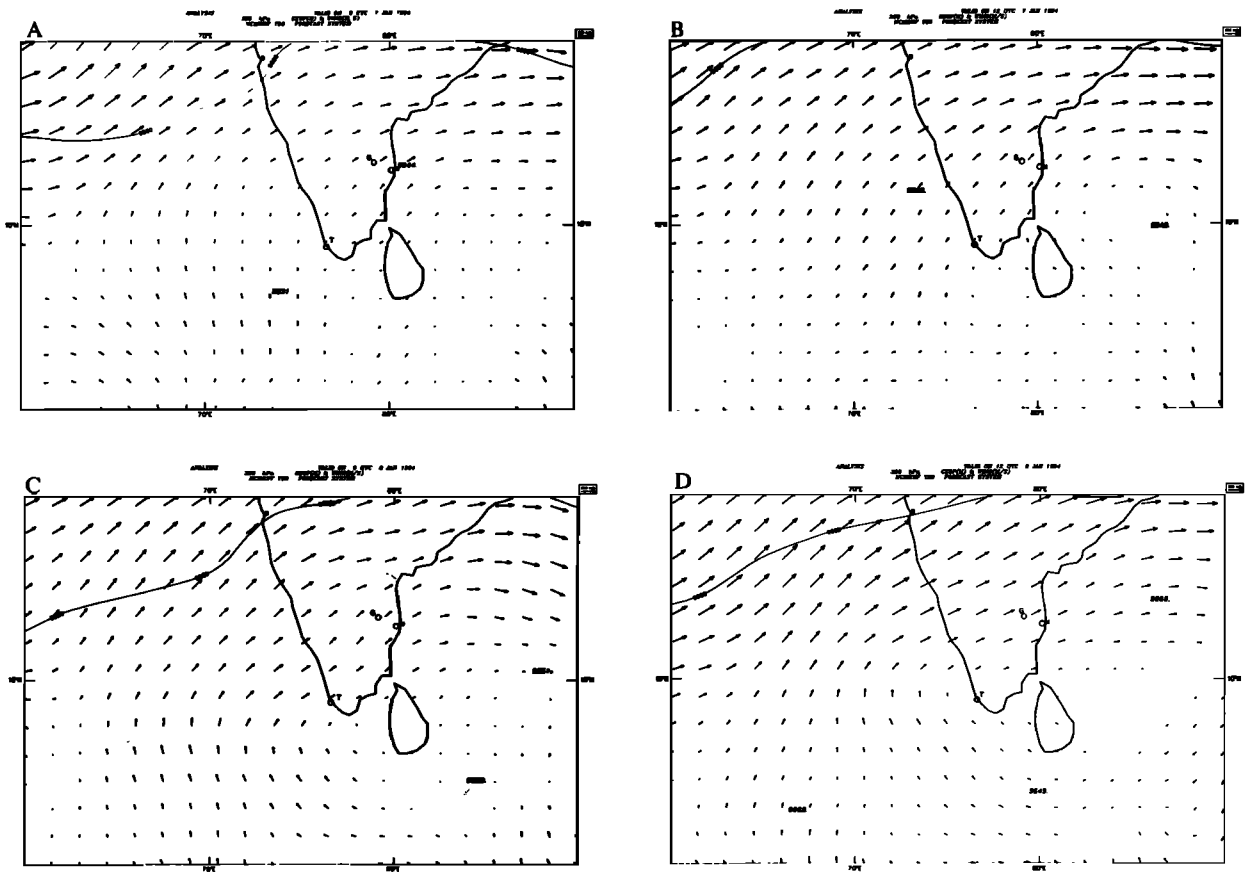

Figure 23. The same as the Figure 20 but at 300 hPa.

likely associated with subsynoptic (meso-alpha) scale features [*Nastrom et al.*, 1989]. Therefore the comparative time series analysis of radar data with weather maps and cross sections based on synoptic radiosonde data suggest that any temporal change in wind vector direction observed by MST radar is not noticeable in synoptic weather charts of 1200 UTC, January 7 and 0000 UTC, January 8, 1994.

The comparative analysis of Figures 16-23 suggests that the synoptic features of the decrease in stratospheric ozone are observed in the integrated stratospheric ozone, but the observed decrease in stratosphere is probably not the result of horizontal advection. It requires large upward vertical wind, which is absent here. In addition, low spatial gradient in the integrated stratospheric ozone surroundings of the Tirupati (13.5°N, 79.2°E) and Trivandrum (8.9°N, 76.6°E) also discards this hypothesis. Therefore the stratospheric ozone may be the result of downward transport, which may increase tropospheric ozone. The easterly wind pattern within 0^0 -10^0N and southeasterly horizontal wind within 10^0-20^0N at 300, 500, and 700 hPa does not strongly support the hypothesis that the increment in tropospheric ozone particularly at the upper troposphere is either the result of horizontal transport of ozone from surroundings (TOR=5-10 DU) to the site of interest (TOR=15-20 DU) or the results of horizontal advection of tropospheric ozone. Generally, the oceanic air mass is poor in ozone (TOR=5-10 DU, see Figures 19a-19d), and therefore the transport over this site by zonal to quasi-zonal wind is probably not the cause of the ozone increase. To gain further insight into the source of air of the region of interest, the forward and back trajectories analysis along isentropic surface is required.

6. Conclusion

The occurrence of tropopause weakening is observed several times on different timescales of different degree

during the period of January 3-8, November 9-16, and December 5-10, 1994. Simultaneous measurements of ozone concentration on January 7-8, November 10, and December 7-8, 1994, have shown intrusion of stratospheric ozone into the troposphere, whereas during January 4-5, 1994, no significant change in ozone concentration is observed during this event. The synoptic features of downward transport of ozone are verified through the decrease in integrated stratospheric ozone and the corresponding increase in tropospheric ozone residual (TOR) using Meteor 3 TOMS and Microwave Limb Sounder (MLS) satellite data. The evidence does not strongly support the hypothesis that increment of tropospheric ozone is due either to its spatial gradient or to horizontal transport by large winds. The transport process of stratospheric ozone into the troposphere across the tropopause may occasionally take place in tropics during the tropopause weakening and can be summarized as follows:

1. The atmosphere comprises dynamical processes of different scales. The nonlinear strong interaction of these processes may generate large-scale instability in the wind field and result in turbulence.

2. The turbulence observed above the tropopause may destroy the stability at the tropopause that normally prevents stratosphere-troposphere exchange. Therefore it results in weakening (disappearance) of the tropopause.

3. Stratospheric air masses descend to the upper tropospheric region through the "weak tropopause" if the magnitude of vertical velocity is low or direction is downward.

4. Ozone is either carried along with this descending air mass or diffuses downward, driven by its own vertical gradient. These two mechanisms can also take place simultaneously.

5. However, it cannot be ascertained at this stage which of the two mechanisms predominates. In both the cases it results in a decrease of ozone concentration from the normal in the stratosphere and an increase in the troposphere with descending of peak height.

Therefore the exchange of ozone during "tropopause weakening" could have a significant effect on the budget of chemical composition, especially for such species as ozone. On the basis of measured NO_x (ground) over the Indian subcontinent, the local production of tropospheric ozone, which may have a role in the increment of tropospheric ozone and its budget, can be calculated using a three-dimensional model. It is out of scope of this discussion, however.

Acknowledgments. We thank the Department of Science of Technology, India, for funding this research. The authors acknowledge the cooperation received from N. SenRoy, DG, IMD, and K. K. Mahajan, RASD, NPL. A large part of data analysis and plotting was based on programs originally developed by V. K. Anandan and Mukund Vaidya, NMRF, Tirupati. The authors acknowledge the help and support of technical staffs of NMRF, Tirupati, and IMD, Trivandrum, while performing the experiments at respective places. One of the authors (T.K.M.) is thankful to U.G.C. for the award of research fellowship. The Arecibo Observatory is part of the National Astronomy and Ionosphere Center, which is operated by Cornell University under a cooperative agreement with the National Science Foundation. Members of the Meteor 3 TOMS experiment and the Ozone Processing Team of NASA Goddard Space Flight Center and GSFC Distributed Active Archive Center (DAAC) are acknowledged for the use of the Meteor 3 TOMS data. The entire processing team of MLS data of UARS as a source of MLS ozone data is gratefully acknowledged.

References

Acharya, Y.B., et al., Indo-USSR Ozonesonde Intercomparison Experiment at Thumba, *ISRO-IMAP-SR-24-85*, 55 pp., Indian Space Res. Org., Bangalore, India, June 1985a.

Acharya, Y.B., et al., Indo-USSR Ozonesonde Intercomparison Experiment at Thumba-Part-II, *ISRO-IMPA-SR-24-85*, 58 pp., Indian Space Res. Org., Bangalore, India, June 1985b.

Attmannspacher, W., and H. Dutch, International ozone sonde intercomparison at the Observatory of Hohenpeissenberg, *Ber. Dtsch. Wetterdienstes, 120*, 47 pp.,1970.

Attmannspacher, W., and H. Dutch, 2nd International ozone sonde intercomparison at the Observatory of Hohenpeissenberg, *Ber. Dtsch. Wetterdienstes, 157*, 64 pp.,1981.

Bamber, D.J., P.G. Healey, B.M. Jones, S.A. Penkett, A.F.Tuck, and G. Vaughan, Vertical profiles of tropospheric gases - Chemical consequences of stratospheric intrusions, *Atmos. Environ., 18*, 1759-1766, 1984.

Bansal, R.K., and S.R.H. Rizvi, A new approach to the analysis problem, in *Advances in Tropical Meteorology, Meteorology and National Development, Proceedings of the National Symposium TROPMET-93*, edited by R.K. Dutta, pp. 23-32, Concept, New Delhi, India, 1993.

Barath, F., et al., The Upper Atmospheric Research Satellite Microwave Limb Sounder instrument, *J. Geophys. Res., 98*, 10,751-10,762, 1993.

Bjerknes, J., and E. Palmen, Investigations of selected European cyclones by means of serial ascents, *Geophys. Norr., 12*(2), 5-62 , 1937.

Brewer, A.W., and J.R. Milford, The Oxford-Kew ozone sonde, *Proc. R. Soc. London, Ser, A, 256*, 470-495, 1960.

Cunnold, D.M., H. Wang, W.P. Chu, and L. Froidevaux, Comparisons between Stratospheric Aerosol and Gas

Experiment II and microwave limb sounder ozone measurements and aliasing of SAGE II ozone trends in the lower stratosphere, *J. Geophys. Res.*, *101*, 10, 061-10,075, 1996.

Dalaudier, F., C. Sidi, M. Crochet, and J. Vermin, Direct evidence of sheets in atmospheric temperature fields, *J.* Atmos. *Sci.*, *51*, 237-248, 1994.

Danielsen, E.F., Stratospheric-tropospheric exchange based on radioactivity, ozone and potential vorticity, *J. Atmos. Sci*, *25*, 502-518, 1968.

Danielsen, E.F., and J. Mohnen, Project Dustorm report: Ozone transport, in situ measurements, and meteorological analyses of tropopause folding, *J.* Geophys. *Res.*, *82*, 5867-5877, 1977.

Dobson, G.M.B., D.N. Harrison, and J. Lawrence, Measurements of the amount of ozone in the Earth's atmosphere and in relation to other geophysical conditions, *Proc. R. Soc. London*, *122*, 456-486, 1929.

Ebel, A., H. Hass, H.J. Jakobs, M. Laure, M. Memmesheimer, A. Oberreuter, H. Geiss, and Y.H. Kuo, Simulation of ozone intrusion caused by a tropopause fold and cut off low, *Atmos. Environ., Part A, 25*, 2131-2144, 1991.

Fishman, J., and P.J. Crutzen, The origin of ozone in the troposphere, *Nature*, *274*, 855-857, 1978.

Fishman, J., P. Minis, and H.G. Reichle Jr., The use of satellite data to study tropospheric ozone in the tropics, *J. Geophys. Res.*, *91*, 14,451-14,465, 1986.

Fishman, J., F.M. Vukovich, D.R. Cahoon, and M.C. Shipham, The characterization of an air pollution episode using satellite total ozone measurements, *J. Clim. Appl. Meteorol.*, *26*, 1638-1654, 1987.

Fishman, J., C.E. Watson, J.C. Larsen, and J.A. Logan, Distribution of tropospheric ozone determined from satellite data, *J. Geophys. Res.*, *95*, 3599-3617, 1990.

Folkins, I., and C. Appenzeller, Ozone and potential vorticity at the subtropical tropopause break, *J. Geophys. Res. 101*, 18,787-18,792, 1996.

Fritts, D.C., and P.K. Rostogi, Convective and dynamical instabilities due to gravity wave motions in the lower and middle atmosphere: Theory and observation, *Radio Sci.*, *20*, 1247-1277, 1985.

Froidevaux, L., J.W. Waters, W.G. Read, L.S. Elson, D. A. Flower, and R.F. Jarnot, Global ozone observations from UARS MLS: An overview of zonal mean results, *J. Atmos. Sci.*, *51*, 2846-2866, 1994.

Froidevaux, L., et al., Validation of UARS Microwave Limb Sounder ozone measurements, *J. Geophys. Res., 101*, 10,017-10,060, 1996.

Gage, K.S., and J.L. Green, Tropopause detection by partial specular reflection using VHF radar, *Science*, *203*, 1236-1240, 1979.

Gage, K.S., and B.B. Balsley, On the scattering and reflection mechanisms contributing to clear air radar echoes from the troposphere, stratosphere, and mesosphere, *Radio Sci.*, 15, 243-257, 1980.

Gage, K.S., W.L. Ecklund, A.C. Riddle, and B.B. Balsley, Objective tropopause height determination using low-resolution VHF radar observations, *J. Atmos. and Oceanic Technol.*, *3*, 248-254, 1986.

Gouget, H., J. Cammas, A. Marenco, R. Rosset, and I. Jonquieres, Ozone peaks associated with a subtropical tropopause fold and with the trade wind inversion: A study from the airborne campaign TROPOZ II over the Caribbean in winter, *J. Geophys.* Res., *101*, 25,979-25,993, 1996.

Herman, J.R., et al., Meteor 3 total ozone mapping spectrometer (TOMS) data products user's guide, *NASA Ref. Publ. 1393*, pp. 1-58, 1996.

Hocking, W. K., Measurement of turbulent dissipation rates in the middle atmosphere by radar technique: A review, *Radio Sci., 20*, 1403-1422, 1985.

Hoskins, B.J., M.E. McIntyre, and A.W. Robertson, On the use and significance of isentropic potential vorticity maps, *Q. J. R. Meteorol. Soc., 111*, 877-946, 1985; (Correction, *Q. J. R. Meteorol. Soc., 113*, 402-404, 1987.)

Jain, A.R., Y. Jaya Rao, P.B. Rao, G. Viswanathan, S.H. Damle, P. Balmuralidharan, and A. Kulkarni, Preliminary observations using ST mode of the Indian MST radar: Detection of signature of tropopause, *J. Atmos. Terr. Phys.*, *56*, 1157-1162, 1994.

Jaya Rao, Y., A.R. Jain, V.K. Anandan, P.B. Rao, G. Viswanathan and R .Arvindan, Some observations of tropical tropopause using ST mode of the Indian MST radar: Multiple stable layer structure, *Indian. J. Radio and Space Phys., 23*, 75-85, 1994.

Larsen, M.F., and J. Rottger, Observations of frontal zone and tropopause structures with a VHF Doppler radar and radiosondes, *Radio Sci., 20*, 1223-1232, 1985.

Mahlman, J.D., Dynamics of transport processes in the upper troposphere, *Science, 276*, 1079-1083, 1997.

McPeters, R.D., et al., NIMBUS-7 total ozone mapping spectrometer (TOMS) data products user's guide, *NASA Ref. Publ. 1384*, pp. 1-84, 1996.

Mohanty, U.C., G.R. Iyengar, S. Basu, E. Klinker, G.H. White, S.F. Milton, and D. Singh, An inter-comparision of medium range prediction of selected features of Asian summer monsoon activity with operational GCMs, in *Proceedings of the WMO International Conference on Monsoon Variability and Prediction,* pp. 351-361, World Meteorol. Org., Geneva,1994.

Nastrom, G.D., J.L. Green, M.R. Peterson, and K.S. Gage, Tropopause folding and the variability of the tropopause height as seen by the Flatland VHF radar, *J. Appl. Meteorol., 28*, 1271-1281, 1989.

Parrish, D.F., and J.C. Derber, The National Meteorological Center's spectral statistical interpolation analysis system, *Mon. Weather. Rev., 120*, 1747-1763, 1992.

Ramanathan, V., and R.E. Dickinson, The role of stratospheric ozone in the zonal and seasonal radiative energy balance of

the earth-tropospheric system, *J. Atmos.* Sci., 36, 1084-1104, 1979.

Rao, P.B., A.R. Jain, P. .Kishore, P. Balmuralidharan, S.H. Damle, and G. Viswanathan, Indian MST radar, 1, System description and sample wind measurements in ST mode, *Radio Sci., 30*, 1125-1138, 1995.

Rastogi, P.K., and J. Rottger, VHF radar observations of coherent reflections in the vicinity of the tropopause, *J. Atmos. Terr. Phys., 44*, 461-469, 1982.

Reed, R.J., The role of vertical motions in ozone-weather relationships, *J. Meteorol.,7*, 263-267, 1950.

Reiter, E.R., M.E. Glasser, and J.D. Mahlman, The role of the tropopause in the stratospheric-tropospheric exchange process, *Geofis. Pura Appl. , 75*, 185-218, 1969.

Rodgers, B.E., J. Stout, J. Steranka, and S. Chang, Tropical cyclone-upper atmosphere interaction as inferred from satellite total ozone observations, *J. Appl. Meteorol., 29*, 934-954, 1990.

Sato, T., Radar principles, *Handbook for MAP*, edited by S. Fukao, 30, 19-53, SCOSTEP Secr., Univ. of Ill., Urbana, 1989.

Shapiro, M. A., A.J. Krueger, and P.J. Kennedy, Nowcasting the position and intensity of jet streams using a satellite-borne total ozone mapping spectrometer, in *Nowcasting*, edited by K.A. Browning, pp. 137-145, Academic, San Diego, Calif., 1982.

Smit, H.G.J., et al., JOSIE: The 1996 WMO international intercomparison of ozonesonde under quasi flight conditions in the environmental simulation chamber at Julich., in *Proceedings of XVIII Quadrennial Ozone Symposium*, edited by R. Bojkov and G. Visconti, 1996.

Sreedharan, C.R., An Indian electrochemic ozonesonde, *J. Phys. E. Sci. Instrum. Sr. 2*(1), 995-997, 1968.

Suhre, K., J.P. Cammas, P. Nedelec, R. Rosset, A. Marenco, and H.G.J. Smit, Ozone-rich transients in the upper equatorial Atlantic troposphere, *Nature, 388*, 661-663, 1997.

Uccellini, L.W., D. Keyser, K.F. Brill, and C.H. Wash, The President's Day cyclone of 18-19 February 1979: Influence of upstream trough amplification and associated tropopause folding on rapid cyclogenesis, *Mon. Weathe. Rev., 113*, 962-988, 1985.

Vaughan, G., and J.D. Price, Ozone transport into the troposphere in a cut-off low event, in *Ozone in the Atmosphere*, edited by R.D. Bojkov and P. Fabian, pp. 415-418, A. Deepak, Hampton, Va., 1989.

Vukovich, M.F., V. Brackett, J. Fishman, and J.E. Sickles II, On the feasibility of using the tropospheric ozone residual for nonclimatological studies on a quasi-global scale., *J. Geophys. Res., 101*, 9093-9105, 1996.

Waterman, A. T., T-Z. Hu, P. Czechowsky, and J. Rottger, Measurement of anisotropic permittivity structure of upper troposphere with clear-air radar, *Radio Sci., 20*, 1580-1592, 1985.

Waters, J.W., L. Froidevaux, G.L. Manney, W.G. Read, and L.S. Elson, Lower stratospheric ClO and O_3 in the 1992 southern hemusphere winter, *Geophys. Res. Lett., 20*, 1219-1222, 1993.

Wofsy, S., J.C. McConell, and M.B. McElroy, Atmospheric CH_4, CO and CO_2, *J. Geophys. Res., 77*, 4477-4495, 1972.

Woodman, R.F., and A. Guillen., Radar observations of winds and turbulence in the stratosphere and mesosphere , *J Atmos. Sci., 31*, 493-503, 1974.

World Meteorological Association, Third WMO intercomparison of the ozonesondes used in the Global Ozone Observing System (Vanscoy, Canada 13-24 May 1991) Global Atmosphere Watch, *Rep. 27*, Geneva, Switzerland, 1994.

Yamanaka, M.D., S. Ogino, S. Kodo, T. Shimomai, S. Fukao, Y. Shibagaki, Y. Maekawa, and I. Takayabu, Inertio-gravity waves and subtropical multiple tropopauses: Vertical wave number spectra of wind temperature observed by the MU radar, radiosondes and operational rawinsonde network, *J. Atmos. Terr. Phys., 6*, 785-805, 1996.

A.K. Bohra, National Center for Medium Range Weather Forecasting, Mausam Bhavan Complex, Lodi Road, New Delhi, India. (e-mail: akb913@ncmrwf.ernet.in)

J.Y.N. Cho, Department of Earth, Atmospheric and Planetary Sciences, Massachusetts Institute of Technology, Cambridge, MA 02139-4307. (e-mail: jcho@pemtropics.mit.edu)

A.R. Jain and P.B. Rao, National MST Radar Facility, P.O. Box 123, Tirupati, A.P., India. (e-mail: nmrf@isro.ernet.in)

T.K. Mandal and A.P. Mitra, Radio and Atmospheric Division, National Physical Laboratory, New Delhi-110 012, India. (e-mail: tuhin@csnpl.ren.nic.in; apmitra@doe.ernet.in)

S.K. Peshin and S.K. Srivastava, India Meteorological Department, New Delhi-110 003, India. (e-mail: peshin@imd.ernet.in)

(Received July 3, 1996; revised November 18, 1997; accepted December 8, 1997.)